

Washington University in St. Louis

Washington University Open Scholarship

All Theses and Dissertations (ETDs)

1-1-2010

Surface Reactivity and Dissolution Rate of Galena: Potential Impact of CO₂ Leakage from Geological Carbon Sequestration on Groundwater Quality

Kathleen O'Malley

Follow this and additional works at: <https://openscholarship.wustl.edu/etd>

Recommended Citation

O'Malley, Kathleen, "Surface Reactivity and Dissolution Rate of Galena: Potential Impact of CO₂ Leakage from Geological Carbon Sequestration on Groundwater Quality" (2010). *All Theses and Dissertations (ETDs)*. 927.

<https://openscholarship.wustl.edu/etd/927>

This Thesis is brought to you for free and open access by Washington University Open Scholarship. It has been accepted for inclusion in All Theses and Dissertations (ETDs) by an authorized administrator of Washington University Open Scholarship. For more information, please contact digital@wumail.wustl.edu.

WASHINGTON UNIVERSITY IN ST. LOUIS
School of Engineering and Applied Science
Department of Energy, Environmental, and Chemical Engineering

Thesis Examination Committee:
Prof. Young-Shin Jun, Chair
Prof. David Fike
Prof. Cynthia Lo

Surface Reactivity and Dissolution Rate of Galena: Potential Impact of CO₂ Leakage from
Geological Carbon Sequestration on Groundwater Quality
by
Kathleen O'Malley

A thesis presented to the School of Engineering
of Washington University in partial fulfillment of the
requirements for the degree of

MASTER OF SCIENCE

May 2010
Saint Louis, Missouri

ABSTRACT OF THE THESIS

Surface Reactivity and Dissolution of Galena: Potential Impact of CO₂ Leakage from Geological Carbon Sequestration on Groundwater Quality

by

Kathleen O'Malley

Master of Science in Chemical Engineering

Washington University in St. Louis, 2010

Research Advisor: Professor Young-Shin Jun

Geological carbon sequestration is one promising solution to mitigating CO₂ emissions and curtailing global climate change. In particular, saline aquifers can store vast amounts of CO₂. This work looks to understand the consequences of any potential leakage from this sequestration, specifically the effect on groundwater quality through the dissolution, precipitation, and surface reactivity of galena. Several saturated, $P_{\text{CO}_2}=1$, and unsaturated CO₂, $P_{\text{CO}_2}=0$, solutions were prepared with varying ionic strengths including 1.0 M NaCl, 0.01 M NaCl, and no NaCl. This study investigated the bulk dissolution rate of galena for both a continuous CO₂ leak system as well as one-time CO₂ leak scenario by analyzing the Pb²⁺ concentration with ICP-MS and Flame-AA. *In-situ* and *ex-situ* AFM experiments were run on cleaved sample to understand and quantify different surface changes on galena. XPS, FTIR, and SEM analysis was also performed to identify the different phases. The dissolution rate of galena in the presence of CO₂ is calculated as well as the mineral phases present. The net dissolution rate of PbS under CO₂ saturated condition ($P_{\text{CO}_2}=1$) is lower than that CO₂ under unsaturated condition ($P_{\text{CO}_2}=0$) and much lower on the (100) surface of galena. Precipitation was dominant in the $P_{\text{CO}_2}=1$ system and the frequency of precipitations increased in the presence of the (111)/(110) surface. The secondary mineral phases can be (PbO), (PbCO₃·2Pb(OH)₂), (Pb₅O(CO₃)₃(OH)₂), or (Pb₂O(CO₃))PbO. The reaction of CO₂ and PbS has a significant effect when in contact with PbS and should continue to be studied to understand the effects of CO₂ leakage.

Acknowledgments

I would like to acknowledge my advisor, Professor Young-Shin Jun, for her help and guidance in exposing me to research and particularly this project and for reviewing this thesis.

Thanks also to the members of my thesis committee, Professor David Fike and Professor Cynthia Lo for their time and expertise. Their comments and insights were extremely useful and greatly improved this work.

I would also like to thank the members of the Environmental Nanochemistry Lab for all of their support and constructive comments. Thanks specifically to Jessica Ray for her friendship and providing a constant source for laughs and encouragement. I'd also like to thank Yandi Hu, Yi Yang, and Dr. Hongbo Shao for their advice and help in the laboratory.

Thanks to Xingyi Deng (NETL) National Energy Technology Lab for measurements and invaluable help with analysis for XPS samples.

I would also like to thank my three sisters, Monica, Andrea, and Emily, for their love and support and Adam for his encouragement, kindness, and superior listening skills.

Kathleen O'Malley

Washington University in St. Louis

May 2010

Dedicated to my dad, William R. O'Malley

Contents

Abstract.....	ii
Acknowledgments.....	iii
List of Tables.....	vii
List of Figures.....	viii
1 Introduction.....	1
1.1 Global Climate Change.....	1
1.2 Geological Carbon Sequestration (GCS).....	2
1.3 Risks of GCS – Potential CO ₂ Leakage.....	5
1.4 Literature Review.....	8
1.4.1 PbS Dissolution and Precipitation of Secondary Mineral Phases.....	8
1.4.2 Surface Reactivity.....	12
2 Experimental Methods.....	14
2.1 Surface Morphology Observations.....	14
2.1.1 AFM – Theory & Modes.....	14
2.1.2 AFM – Experimental Preparation & Use.....	16
2.1.3 SEM – Principle.....	17
2.2 Precipitation Identification.....	17
2.2.1 FTIR - Principle.....	17
2.2.2 XPS - Principle.....	18
2.2.3 Experimental Preparation & Use.....	19
2.3 Aqueous Chemistry.....	19
2.3.1 ICP-MS - Principle.....	20
2.3.2 Flame-AA - Principle.....	20
2.3.3 Experimental Preparation & Use.....	21
2.4 Surface Area.....	21
2.4.1 BET.....	22
2.5 Experimental Design.....	22
2.5.1 AFM <i>in situ</i> experiment.....	22
2.5.2 Single leak experiment.....	23
2.5.3 Continuous leak experiment.....	23
2.5.4 AFM <i>ex situ</i> experiment.....	24
3 Experimental Results.....	26
3.1 <i>In situ</i> AFM Results.....	26
3.1.1 Concentrations.....	26
3.1.2 Surface Morphology.....	27

3.2	Single leak Results	27
3.2.1	Concentrations & FTIR.....	27
3.3	Continuous leak Results	30
3.3.1	Concentrations & FTIR.....	30
3.4	Unsaturated CO ₂ – P _{CO₂} =0	34
3.4.1	Unsaturated CO ₂ Condition (P _{CO₂} =0).....	34
3.4.2	Different Planes – (100) and (110)/(111)	35
3.4.3	Cleavage Planes: (111) & (111)/(110) Surface.....	37
3.5	SEM Results.....	39
3.5.1	Crystal Samples	39
3.5.2	Powder Samples.....	41
3.6	XPS Results.....	42
4	Discussion	47
4.1	Effects of Aqueous Chemistry & Ionic Strength	47
4.2	Dissolution Rates	49
4.3	Surface Plane Reactivity	51
4.4	Precipitation Identification	53
4.5	Environmental Implications.....	55
5	Conclusions & Future Work.....	56
5.1	Conclusion.....	56
5.2	Future Work.....	57
Appendix A	References for Peak Matches	59
A.1	Peak Matches for FTIR.....	59
A.2	Peak Matches for XPS.....	60
References	61
Vita	65

List of Tables

Table 1.1: Geological Sequestration Field Site Conditions	4
Table 3.1: Secondary Mineral Precipitation Analysis	37
Table 3.2: <i>In situ</i> Flow-thru in AFM fluid cell Dissolution Rates	49
Table A.1: Peak Matches for FTIR.....	59
Table A.2: Peak Matches for XPS	60

List of Figures

Figure 1.1: Overview of Geological Storage Options	2
Figure 1.2: Potential Pathways for CO ₂ Leakage	5
Figure 1.3: Eh-pH diagram for the Pb-CO ₂ -H ₂ O system	11
Figure 2.1: AFM Schematic Diagram	15
Figure 2.2: AFM Modes: Contact and Tapping	16
Figure 2.3: SEM Schematic Diagram.....	17
Figure 2.4: FTIR Schematic Diagram.....	18
Figure 2.5: XPS Schematic Diagram.....	19
Figure 2.6: ICP-MS Schematic Diagram	20
Figure 2.7: Flame-AA Schematic Diagram	21
Figure 2.8: AFM <i>in situ</i> Experimental Setup	23
Figure 2.9: Experimental Schematic for Single and Continuous Leak Experiments.....	24
Figure 2.10: <i>Ex situ</i> AFM Experiment	25
Figure 3.1: AFM <i>in situ</i> Concentration Results.....	27
Figure 3.2: Single-leak: Pb ²⁺ Concentration vs. Time	28
Figure 3.3: Single leak FTIR Absorption Spectra	29
Figure 3.4: Continuous leak: Pb ²⁺ Concentration vs. Time.....	31
Figure 3.5: Continuous leak FTIR Absorption Spectra	31
Figure 3.6: FTIR Absorption Spectra Comparison: CO ₂ Saturated.....	33
Figure 3.7: AFM Image of Dissolution, P _{CO₂} =0.....	34

Figure 3.8: AFM Image of Precipitation (100), $P_{CO_2}=1$	35
Figure 3.9: AFM Image of Precipitation (100)+(111)/(110), $P_{CO_2}=1$	36
Figure 3.10: AFM Image of Rough (111)/(110) Surface.....	38
Figure 3.11: AFM Image of (111) Surface	39
Figure 3.12: SEM Image: (100) Surface, $P_{CO_2}=0$	40
Figure 3.13: SEM Image: (100) Surface, $P_{CO_2}=1$	40
Figure 3.14: SEM Image: Powder Surface, $P_{CO_2}=0$	41
Figure 3.15a: SEM Image: Powder Surface, $P_{CO_2}=1$	41
Figure 3.15b: SEM Image: Powder Surface, $P_{CO_2}=1$	42
Figure 3.16: XPS Results: Pb 4f Spectra	43
Figure 3.17: XPS Results: S 2p Spectra	44
Figure 3.18: XPS Results: C 1s Spectra	44
Figure 3.19: XPS Results: O 1s Spectra	45
Figure 4.1: (100) Cleavage Plane	52
Figure 4.2: (111) Cleavage Plane	52

Chapter 1

Introduction

1.1 Global Climate Change

Global climate change refers to the change in weather or frequency or intensity of weather over a long period of time. Anthropological climate change is the climate change attributed to the behavior of humans and has been speculated about since the 1950's [1]. Evidence supporting this trend has accumulated over the years and the role of greenhouse gases in the general increase in the surface and ocean temperatures of Earth is generally well-accepted. The potential impact of this phenomenon has resulted in the establishment of the Intergovernmental Panel on Climate Change (IPCC) in 1988 to publish and publicize the current research on climate change [2]. The IPCC report issued in 2007 highlighted the potential adverse effects that climate change may have if left unattended to including extreme variations in traditional weather patterns and the increased melting of polar ice caps with a corresponding rise in ocean sea levels, among other potentially irreversible effects [2]. There are many mitigation strategies, for both short and long-term goals, proposed to begin to reduce the extent and impact of greenhouse gas emissions. Advancing efficiency in many processes across many industries is a high priority; developing and implementing renewable energy sources is also an area of extensive research and potential; and geologic carbon sequestration (GCS) is a promising research initiative to store vast amounts of one of the most prevalent greenhouse gases, CO₂, underground.

1.2 Geologic Carbon Sequestration

Geologic carbon sequestration (GCS) is the second phase of the mitigation effort known as carbon capture and storage (CCS). Geologic carbon sequestration is an important mitigation option as it can store large scale quantities of CO₂ and has the potential to make an immediate impact with quick implementation. GCS is divided into two main categories: terrestrial and geologic sequestration. Terrestrial sequestration involves enhancing the amount of CO₂ absorbed by plants and more importantly soils where it can be stored for long periods of time. Efforts to plant trees, introduce no-tilling farming, and support forest preservation have all been done on behalf of terrestrial sequestration. The other viable option for long-term carbon sequestration is geological storage, which looks to utilize the geologic formations of the earth to store large amounts of CO₂ under the surface. Geologic sequestration has three main divisions within it, seeking to use CO₂ with enhanced oil recovery (EOR), in unmineable coal beds, or in deep, saline aquifers.

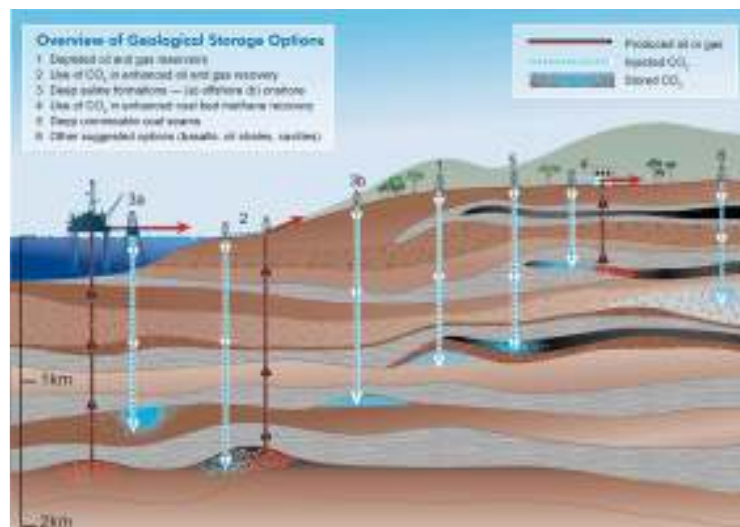


Figure 1.1 Overview of Geological Storage Options[3]

Among those options in Figure 1.1, deep saline aquifers are one of the most promising strategies. Positioned at depths ranging from 3,500-8,000 ft, deep saline aquifers have the potential to store vast amounts of CO₂ emissions. Improvements in the understanding about geologic sequestration may help to facilitate the deployment of geologic sequestration in the United States.

The Department of Energy has funded seven regional partnerships across the United States including the Big Sky Regional Carbon Sequestration Partnership (Big Sky)[4], Midwest Geological Sequestration Consortium (MGSC)[5], Midwest Regional Carbon Sequestration Partnership (MRCSP)[6], Plains CO₂ Reduction Partnership (PCOR)[7], Southeast Regional Carbon Sequestration Partnership (SECARB)[8], Southwest Regional Partnership on Carbon Sequestration (SWP)[9], and West Coast Regional Carbon Sequestration Partnership (WESTCARB)[10] to investigate the viability of various mitigation schemes including CO₂ sequestration. These partnerships have implemented deep saline aquifer carbon sequestration in various stages across the United States. Appropriate saline aquifer sites are determined by characteristics including porosity, permeability, cap rock thickness, and other geological features. Table 1.1 compiles all the geological settings for these regional partnerships.

Among the site selection criteria, porosity and permeability are two characteristics particularly important in regards to leakage from GS sites. Porosity is the measure of the void or pore spaces in a material and is usually given as a percentage. An appropriate cap rock needs to be designated for a stable saline aquifer, as this is one of the important barriers to keeping CO₂ captured within the earth. Permeability is a measurement of the ease in which liquid or fluids can flow through the porous rock. Saline aquifers need relatively low porosities, around 10-20%, and low permeability, around 20 mD, and at least a cap rock thickness of 500 ft. The stability and integrity of the aquifers chosen are extremely important to ensure the long-term success of CO₂ sequestration as well as the extent and impact of any potential CO₂ leakage.

Table 1.1 Geological Sequestration Settings

Group	Pressure	Temperature	Salinity	Porosity	Permeability
Big Sky			1,000-300,000 ppm	10-15%	
MGSC	2,400-4,300 psia: 100-500 psia: 0.433 psi/ft M=1000-1200 psi: 300- 850 psi	120-180 °F: 55-80 °F: 62°F at 100 ft 1F/100ft M=85-90: 80°F	20,000-180000 ppm	<20%, 10%: 1-3%: 16- 19%	<10mD: 50-70 mD: <20: 34-67 mD
MRCSP	1,000-1,100 psi		111,000 mg/L	sandstone: 3-30%, shale: -10%, sand and gravel 25-50%: 10%: 14%	42 mD: 10-200+mD: 0.1 mD, 10-100 mD, 100- 1000 mD
PCOR	0.46 psi/ft: 100 psia at 400 ft, 400 psia at 1,250 ft	15°F/1,000ft+60°F	100-800 ppm	20% upper, 6-36% Powder River Basin, 0.1-13,000 mD mean 915 mD	20-130 ft/day, 10 ⁻¹³ to 10 ⁻¹⁰ ft ² intrinsic
SECarb	8.4 MPa	114.8 °F	<10,000 mg/L		22 md: decreased with depth 1mD at 500 m, 10 mD at 350 m
SWP	1,245-9,400	107-275	3055-100000	4-22%: 0-24%: 0-18%	0-121 mD: 0.1-300 mD
WestCarb	1500 psi, 21.30MPa, 8.4MPa	129 F, 114 F		10-40%	22 mD, .2-10,000mD

1.3 Risks of GCS – Potential CO₂ Leakage

CO₂ leakage from deep, saline aquifers is the one of the concerns that the deployment of GCS needs to resolve. There are many ways that CO₂ could leak from geological formations within the Earth and it is very important to consider these options and understand what effect such leaks could have to understand the risks involved in carbon sequestration and understand what impact leaking CO₂ may have on groundwater quality.

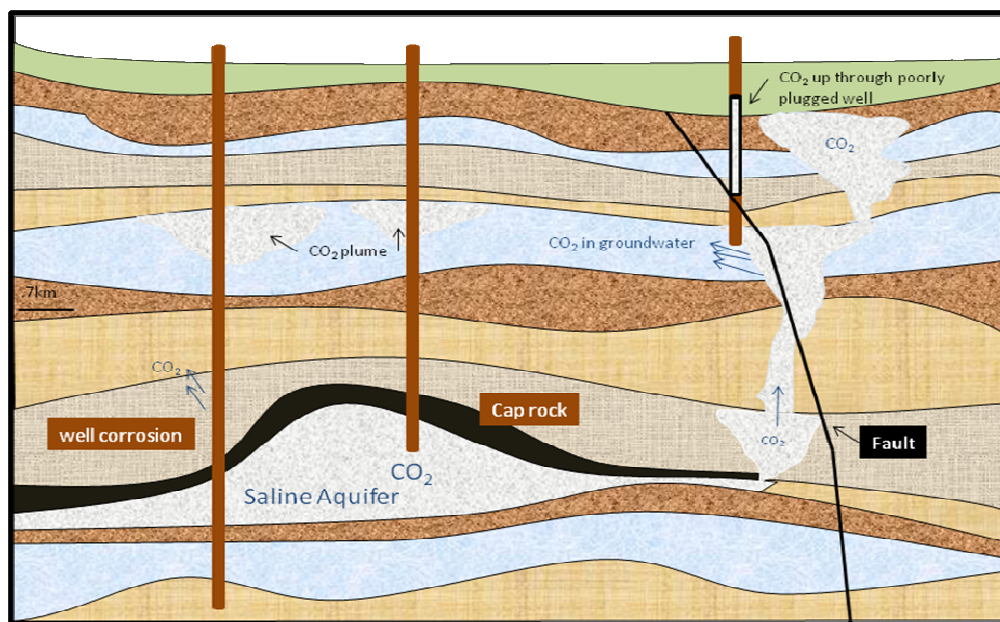


Figure 1.2 Potential Pathways for CO₂ Leakage¹

Choosing the GCS sites is the most important consideration for the operation of geologic sequestration. First, seismic activity is one source of concern that could alter the arrangement of rock layers that make an aquifer conducive for carbon sequestration storage. Any shift in the carefully selected rock formations could provide continuous pathways for CO₂ to reach depths close to the surface and impact groundwater. Weaknesses in old piping and wells are another concern for monitoring leaking CO₂ as they could provide sources for CO₂ leakage until fixed. Any soft spots in the piping are dangerous flaws reducing the reliability of the seals of the saline aquifer and should be monitored and analyzed to ensure quality. In addition, geochemical reactions with CO₂

¹ Image for illustration purposes only. Not intended to depict specific rock layers.

and the rock in the saline aquifer at the injection sites have unknown effects on the integrity of the saline aquifer and could result in increasing CO₂ leakage from these points. Reactions between CO₂ and the rock boundaries of the saline aquifer as well as the effects of the increasing acidification of the saline aquifer are important mechanisms to observe. While the benefit of geologic sequestration of supercritical CO₂ is obvious, and evidence is accumulating that geologic CO₂ sequestration is technically feasible, leakage of CO₂ during injection and long-term storage to overlying drinking water sources may occur and impact public health and environment [11-13]. Despite the various precautions that will surely be developed and implemented to protect against the various liabilities mentioned above, zero leakage of CO₂ from GCS may not be possible, as some amount of CO₂ will leak naturally from the saline aquifer at some measurable level because of the buoyant nature of CO₂ and inevitable weakening of the various seals. The wells and seals utilized for CO₂ sequestration are also a significant consideration in ensuring the successful implementation of GCS.

The U.S. Environmental Protection Agency (EPA) Underground Injection Control (UIC) program issues permits for EOR projects and other injection operations within one of five injection well classes under the Safe Drinking Water Act. Recently, the U.S. EPA proposed to modify the UIC program to create a new class of wells (Class VI) for geologic sequestration projects and establish minimum technical requirements for sequestration operations [14]. Under this proposal, EOR projects are expected to remain in the Class II category, while hybrid EOR-GS operations would be regulated as Class II wells until CO₂ injection for EOR is complete. Class VI permits will be issued for further injection to support long-term GS [14, 15]. Introducing a new class of wells provides a more well-defined tool for safeguarding the underground sources of drinking water. In order to successfully utilize the new class of wells, the more accurate reaction rates at CO₂-rock-water interfaces in underground sources of drinking water (USDWs) is required to apply the scale-up modeling and field site applications. Analog studies of geologic environments containing large, concentrated amounts of CO₂ have shown that leakage processes are inherent in CO₂ sequestration [16]. It has been estimated that allowing 1% leakage of stored CO₂ over 100 years is necessary for sequestration to be

viable [17]. Any CO₂ that leaks from deep saline aquifers could potentially influence water quality and underground sources of drinking water (USDWs).

Potential CO₂ leakages could see CO₂ continue to move up through the earth's geologic layers until it reaches groundwater levels and began to impact drinking water. The levels of CO₂ reaching groundwater sources is important to consider and monitor as this could have very adverse effects on the health of human and animal populations. Increasing CO₂ levels is likely to lower the pH of groundwater sources, perhaps significantly if large quantities were able to find pathways to the surface. The pH value is an important parameter in aqueous chemistry and while no enforceable drinking water regulations exists for monitoring pH, the accepted range for healthy drinking water is a pH between 6.5-8.5. Many rocks in this area of research, including the source of the particular rocks in this experiment, the Illinois Basin, are composed of many different minerals including the mineral of interest in our study, galena, which have the potential to introduce lead into the system and groundwater [18]. One of the most common natural sources of lead sulfide, galena is found in a variety of places including the Mississippi Valley type deposits in Missouri and in the Driftless Area of Illinois, Iowa, and Wisconsin [19]. An increasingly acidic groundwater source could result in increasing concentrations of these harmful elements. Another parameter to consider in relation to leakage from CO₂ sequestration sites is salinity and the ionic strength of solution. There is data that shows very high salinities expected in different areas of GCS, including the Illinois Basin [20]. The salinity of deep saline aquifers is of note because the effect of ionic strength is important in considering geochemical reactions because minerals tend to be more soluble in concentrated salt solutions rather than dilute ones [21]. Unhealthy amounts of lead present and released into the water supply is a major concern, and the processes related to the reactions that create this scenario must be understood to assess the risks of carbon sequestration and storage and its overall safety. Because aqueous Pb²⁺ has a maximum contaminant level (MCL) of only 15 µg/L according to U. S. EPA regulation, an understanding of the dissolution and precipitation rate of galena in the presence of CO₂ is crucial [22]. Investigations into

these mechanisms at varying levels of CO₂, ionic strength, and various cleavage planes will help gauge the impact of leaking CO₂ on water quality.

This thesis investigated the effects of CO₂ on drinking water quality using a variety of methods including atomic force microscopy (AFM), inductively coupled-plasma mass spectroscopy (ICP-MS), X-ray photoelectron spectroscopy (XPS), flame atomic absorption spectrometry (Flame-AA), and Fourier-transform Infrared spectroscopy (FTIR). AFM images of the surface will be used to observe precipitation formation and other surface changes. Dissolution rates will be observed and heavy metal ions, aqueous Pb²⁺, concentrations monitored with time. The effect of CO₂ on the pH of this system and its impact on the reactions occurring were examined. Experiments to investigate the influence of various galena surfaces on the reactivity of galena and a continuous-flow and single-leak simulated experiment were performed. A holistic understanding of water-rock-CO₂ reactions at the groundwater level will help elucidate the more relevant geochemical reactions, understand potential impacts of GCS leakage, and design appropriate remediation techniques.

1.4 Literature Review

Galena, PbS, is a major source of lead in natural environments and quite ubiquitous, particularly in Missouri where it has the distinction of being the state mineral. It is a good mineral to study because there are several prior experiments conducted on the dissolution of galena, which provide necessary background information and because galena provides a flat surface. It is also environmentally relevant as the monitoring of aqueous lead concentrations is very important.

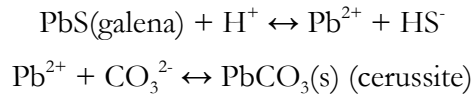
1.4.1 PbS Dissolution and Precipitation of Secondary Mineral Phases

The dissolution rates of minerals, particularly galena, in deep underground saline aquifers are presumed to increase with increased CO₂ concentrations. Leaking CO₂ can induce pH changes and the solubility of trace metals, increasing their concentrations. A

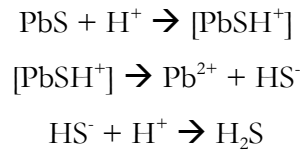
geochemical transport model showed the difference between Pb^{2+} concentrations in a poorly-buffered (galena and quartz system) and well-buffered (galena and calcite system), where Pb^{2+} concentrations levels exceeded safe levels in the non-buffered system while well-buffered levels were within acceptable levels [13]. The simulation in this article was handicapped by the accuracy of thermodynamic and kinetic information data. Additional studies on the issue by Zheng and Apps based on the TOUGHREACT code have found different results than Wang and Jaffe [23]. In a report by Zheng, the concentration of Pb^{2+} in groundwater supplies was below the MCL. Adsorption, rather than dissolution was found to be dominant mechanism, resulting in much lower concentrations in solution [24]. Further information on the mineral dissolution kinetics to more accurately predict the behavior of heavy metals and the quality of groundwater would be ideal. The discrepancies in these two works suggest a need for experimental data to better quantify the mechanisms occurring in this system. Other studies conducted have noted the importance of quantifying changing trends in porosity and permeability in the aquifer and cap rock [25, 26]. It also confirmed again the decrease in pH from CO_2 dissolving into H_2CO_3 , HCO_3^- , and CO_3^{2-} and noted the impact of the buffering capabilities of the aquifer system [27]. The effects of co-contaminants on the integrity of geological storage systems are particularly interesting as the introduction of H_2S and SO_2 might lower the pH of the system below buffering limits, having a more profound impact on the system. An understanding of the basic interaction between CO_2 -rock-water will help provide insight into these processes and assist in geochemical transport models.

The dissolution of Pb^{2+} from galena is a very important aspect of this investigation as Pb^{2+} toxicity makes it imperative to limit its concentration in groundwater. The dissolution of PbS in water and oxidizing conditions has been extensively studied. In PbS- H_2O system reviews, it was shown that the products formed from oxidation are more soluble than galena, so oxidation and dissolution will probably be closely linked [28]. It was also reasoned that the pH of the oxidizing fluid and surface chemistry would play a large role in the oxidation products and reactions [28]. The introduction

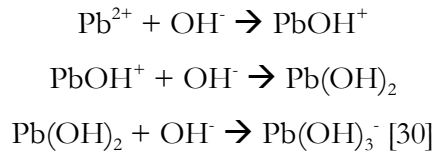
of CO₂ into this equation and its effect on dissolution and precipitation could be expressed with the following equations:



The reaction of HS⁻ is interesting as it can react with other species in the system. A study on the dissolution kinetics of galena in acid NaCl solutions found the reaction mechanism for dissolution to follow these three steps:



The species [PbSH⁺] denotes a surface complex formed by the adsorption of H⁺ onto the galena surface [29]. The actual species this denotes has not been convincingly determined. The influence of lead ions on the dissolution of galena and the growth of colloidal projections on the galena surface has been rationalized by the following equations:



The dissolution and precipitation of Pb²⁺ induced by CO₂ leakage from GCS site is essential to providing a fundamental understanding of this system and the mechanisms that are studied in this work. Quantum chemical calculations have helped shed some light on the subject to assess the thermodynamic favorable reaction mechanism from (100) planes in galena [31]. The addition of protons onto S atoms was found to be energetically favorable thus resulting in a dissolution scheme where Pb²⁺ was replaced by H⁺. The dissolution of protonated S atoms unlikely, the formation of a Pb-deficient, S-rich surface is expected [31]. As evident by the various options presented above, the oxidation and dissolution of PbS is a complicated mechanism and not entirely understood, especially as to how the introduction of CO₂ may affect this progression.

In addition to FTIR, SEM, and XPS analysis, useful information can also be gleaned from the relationships found on an Eh-pH diagram which maps out possible stable phases of an aqueous system.

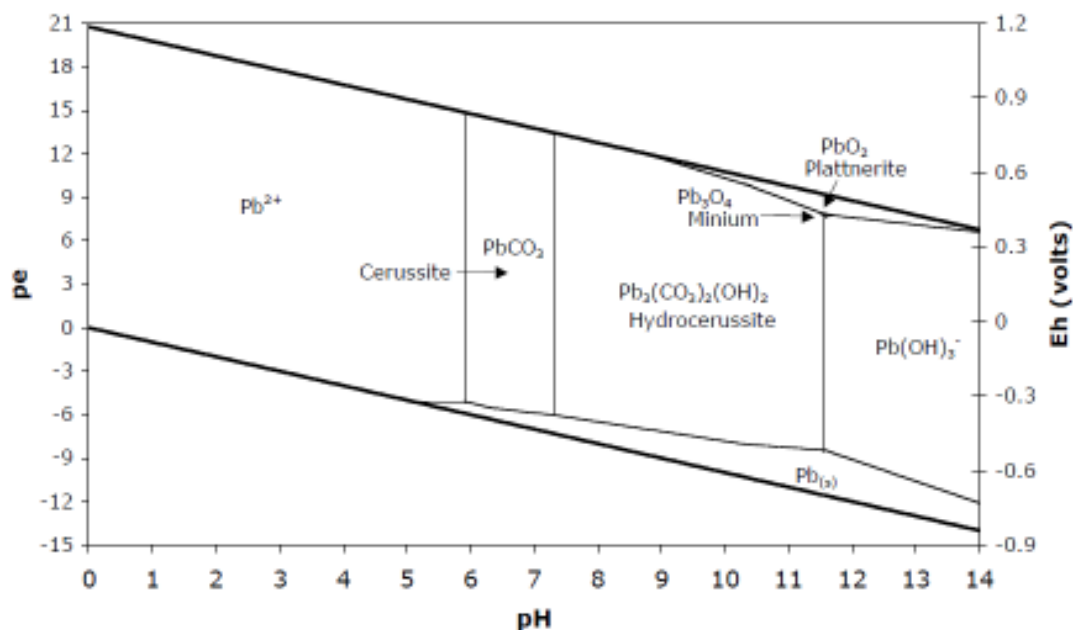


Figure 1.3 Eh-pH diagram for the Pb-CO₂-H₂O system: 25° C and 1 atm, [Pb] = 10⁻⁶ M, and [CO₃]_{Total} = 10⁻² M [32].

This diagram is based on low CO₃ concentration and low Pb concentration of 10⁻⁶ while the initial Pb concentration in our system is 2x10⁻³ M. Therefore, the prediction based on this diagram will not be accurate. However, this Eh-pH diagram could help provide an insight into what species may be available and stable in general systems.

The dissolution rate of galena is closely linked with the formation of precipitation on the galena surfaces. While Pb²⁺ ions may dissolve from the surface of galena, these aqueous Pb²⁺ ions may also adsorb once more to the surface of galena as specific species. There have been several articles on this reaction already though there is still some uncertainty in the literature as to what mineral species are forming on the surface of galena and how they are forming. Nowak and Laajaelhto's XPS study on the oxidation of galena looked at the formation of sulfoxy species. They determined that the adsorption of sulfoxy species to lead sulfide's surface was rather weak and probably replaced by carbonate [33]. The intermediate products formed from galena oxidation

are oligosulfide species which are quite reactive and could form elemental sulfur or sulfoxy species. The introduction of CO_2 could interact with the sulfide sulfur and result in some precipitation on the surface. In a different study, looking at acidic conditions of $\text{pH}=3$, AFM *in situ* studies were conducted and analyzed. These experiments resulted in the formation of a layer of sulfur on the surface of galena and the precipitation of PbSO_4 [34]. Evidently, knowledge of the secondary mineral phase formation is important and a clear understanding lacking for the reaction system of interest in regards to GCS.

1.4.2 Surface Reactivity

Dissolution and precipitation of galena could be closely related to the exposed surface structure to the aqueous condition, therefore the other focus of this report deals with the surface reactivity of galena. There has been some work done that suggests, that for galena, different faces have different reactivity. In particular, Hochella et al. reported that the smooth (100) plane has been shown to dissolve slower than the (111) and (110) faces of galena in non-oxidative dissolution [35]. The reactivity of galena in anoxic, acidic conditions has been investigated and has provided insights on the effect of size and aggregation on galena's reactivity. The dissolution of galena is observed to be favored for nanocrystals of galena as compared to the bulk system [35]. The surface area of nanocrystals is much higher and the presence of (110) and (111) faces are more prevalent and can more greatly affect the dissolution rate [35]. It has also been shown that step defects on galena affect the surface reactivity [36]. Dissolution and precipitation on galena's surface has been closely linked and the potential precipitates on galena should be identified. In an *in situ* oxidative dissolution experiment on the (100) plane the main species were identified for several pHs. For a $\text{pH}=1$, PbO and PbS-PbSO_4 were the main species after 24 and 48 hours. For a $\text{pH}=4.6$, the main species were PbS and SO_3^{2-} [37]. However, there is no study to investigate the secondary mineral phase precipitation at $\text{H}_2\text{O-CO}_2\text{-PbS}$ reactions under high concentration of aqueous CO_2 and high salinity and the potential effects on reactivity that accompany changing the plane of the galena surface exposed to solutions.

This thesis aims to address the several scientific questions concerning the reactions at CO₂-H₂O-PbS interfaces. The dissolution and precipitation rate of galena are important processes to understand and quantify and are a major goal in this report. This thesis also looks to understand the surface reactivity of galena on different crystal planes and as well as the effect of changing the salt concentration of the CO₂ saturated solutions. These scientific questions will be addressed through experiments monitoring aqueous Pb²⁺ concentrations and observing surface morphology changes on galena's surface.

Chapter 2

Experimental Methods

This chapter describes the experimental approach and methods used to investigate the scientific questions posed in this thesis. The surface reactivity and dissolution rate of galena was investigated using atomic force microscopy (AFM), flame atomic absorption spectroscopy (Flame-AA), inductively coupled plasma mass spectrometry (ICP-MS), Fourier-transform infrared spectroscopy (FTIR), scanning electron microscopy (SEM), and x-ray photoelectron spectroscopy (XPS).

2.1 Surface Morphology Observations

The morphology changes on the surface of reacted PbS samples is an important element to broadening our understanding of the system in question since surface images can be obtained to show evidence of dissolution or precipitation. It can also provide quantitative (height and depth) and qualitative (shape of precipitations) information about galena's surface. Surface morphology changes on the nanometer and micrometer scale were monitored using both contact and tapping modes of the AFM as well as with SEM images.

2.1.1 AFM – Principle & Modes

The AFM was developed after the invention of scanning tunneling microscopy to allow for imaging of materials that were not conductors. It is a high-powered microscope that has resolution down to a few nanometers, providing images thousands of times better than typical optical microscopy including TEM and SEM. It is especially useful for imaging the surfaces of materials and is at the forefront of investigating and imaging nanoscale systems. The AFM uses a piezoelectric scanner, diode laser, mirror, and

cantilever tip coupled with the appropriate computer software to image the surface of a specific sample. The cantilever tip is kept at a constant force and the measure of how the tip is deflected as it moves across the surface is what allows for measurement. The flow of information in the AFM is shown below as the laser is reflected off the cantilever tip to a mirror before being directed to a photodetector. The AFM allows us, by balancing various forces including chemical bonds, Van der Waals and repulsive forces, and electrostatic repulsion, to measure the surface of the sample including dissolution pits and precipitation morphology.

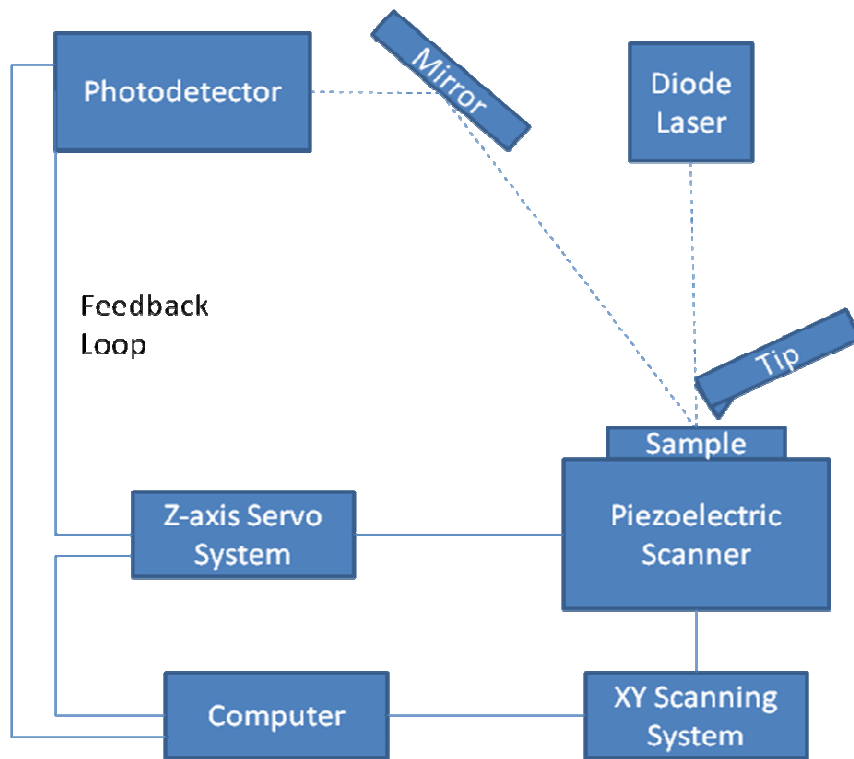


Figure 2.1 AFM Schematic Diagram

The AFM has two commonly used modes: contact and tapping mode. There are advantages and disadvantages to each operating mode and require slightly different operation. Contact mode works by keeping the tip in contact with the surface always and is often easier to operate and can provide good images of the surface as long as the sample is strong enough to withstand the force of the tip on its surface and potential precipitations strong enough to adhere to surface firmly and are not affected by the tip

force. Contact mode yields information on the height, deflection error, and friction readings of the sample. Tapping mode uses oscillations of the tip to generate similar information on height, width, and phase. Tapping mode would be more beneficial for smaller sizes, in particular, for nanoparticles or soft materials observations.

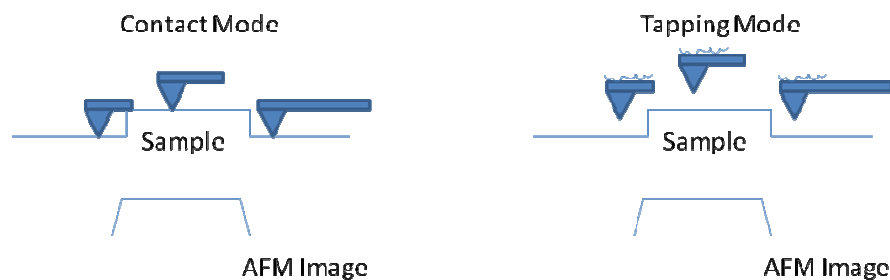


Figure 2.2 AFM Schematic Modes: Contact and Tapping

2.1.2 AFM – Experimental Preparation & Use

Several procedures were implemented to ensure the proper use of the AFM (Veeco Instruments). An *ex situ* and *in situ* experiment were performed and investigated using the AFM. *In situ* samples were prepared by cleaving 1mm x 1mm x 1mm samples and placing them securely on dental wax before using the *in situ* AFM fluid cell. *Ex situ* samples were prepared for AFM imaging by placing cleaved samples onto a piece of double-sided tape. Each sample was analyzed with the AFM cantilever tip in both contact and tapping modes. Galena samples were freshly cleaved and examined with the AFM microscope before reaction to ensure fresh and similar surfaces for each run. After reaction, each sample was washed with DI water and dried by flushing with high purity N₂. All height, amplitude, and phase contrast images of each dried galena sample were collected simultaneously under ambient laboratory conditions in AFM tapping mode. Probes were 125 μm long, with phosphorus (n) doped silicon tips (a nominal tip radius of 10 nm, MPP-11100-10, Veeco probes). The images were collected with a proportional gain of 0.5513, integral gain of 0.2213, drive frequencies of 250-300 kHz, typical spring constants of 20-80 N/m and at a scan rate of around 1.29 Hz. Topography features were measured using Nanoscope 7.20 software [38].

2.1.3 SEM – Principle

The scanning electron microscope (SEM) was first developed in the 1930's and provides 10-500,000 times magnification of sample images. SEM works in a vacuum by scanning a sample surface with a high-energy beam of electrons which interact with the atoms of the sample to produce signals that relay information about the surface topography as well as composition and electrical conductivity. The SEM consists of a column, which generates electrons, a specimen chamber, where the sample is placed, an EDS Dewar to house liquid nitrogen, and a secondary electron detector.

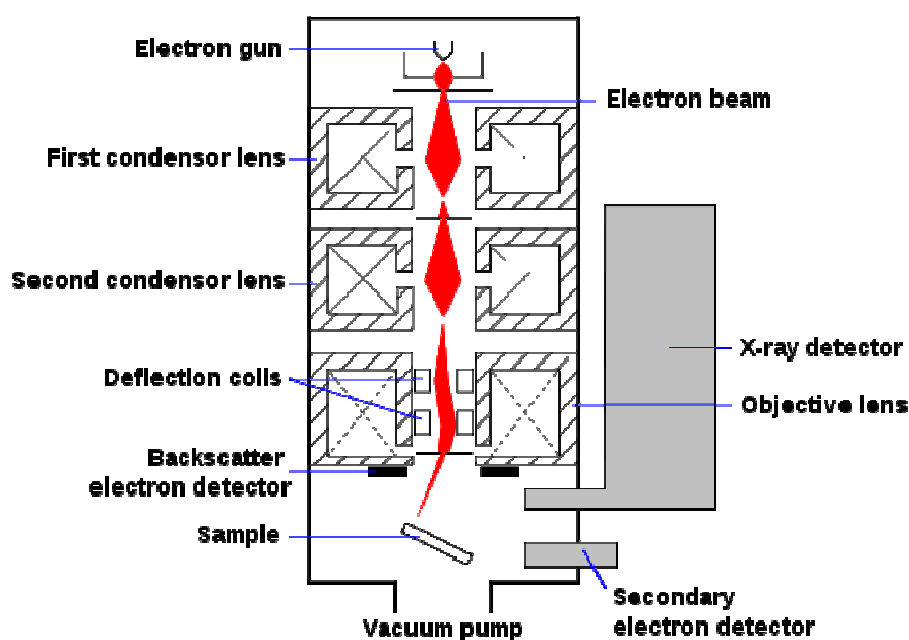


Figure 2.3 SEM Schematic[39]

2.2 Precipitation Identification

The identification of precipitation on the surface of galena after reaction with $\text{CO}_2\text{-H}_2\text{O}$ is a very important facet to the scientific questions addressed in this thesis. FTIR and XPS were used to investigate the secondary mineral phase formation on galena.

2.2.1 FTIR – Principle

FTIR (Fourier transform infrared spectroscopy) is used because it is a non-destructive and provides precise, quick measurements, which can provide chemical bonding information in the samples. FTIR operates by passing infrared radiation through a sample. This radiation is either absorbed or transmitted by the sample. The absorbance spectra that results can be analyzed to discover the molecular elements produced by the reaction. FTIR consists of a source for emitting the infrared energy which is sent through a sample for analysis before being collected on a detector and sent to a computer.

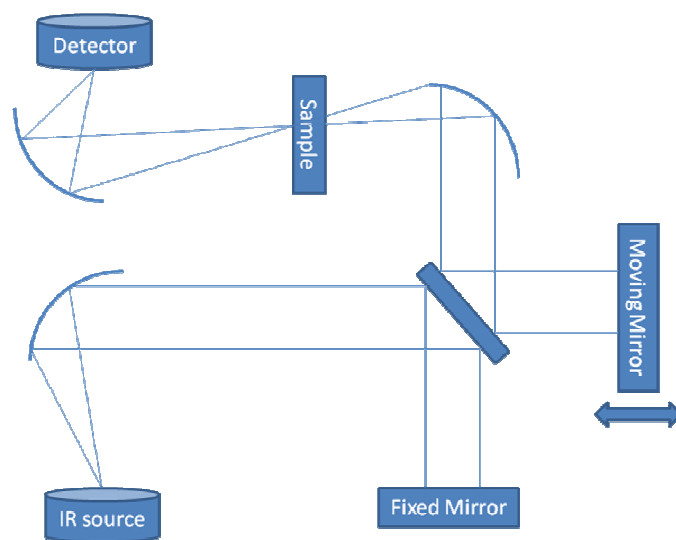


Figure 2.4 FTIR Schematic

2.2.2 XPS – Principle

X-ray photoelectron spectroscopy is an important surface chemical analysis technique that can provide information about elemental composition and oxidation state of the sample surface. XPS works in ultra-high vacuum conditions by irradiating a sample with x-rays while measuring the energy and number of electrons that escape.

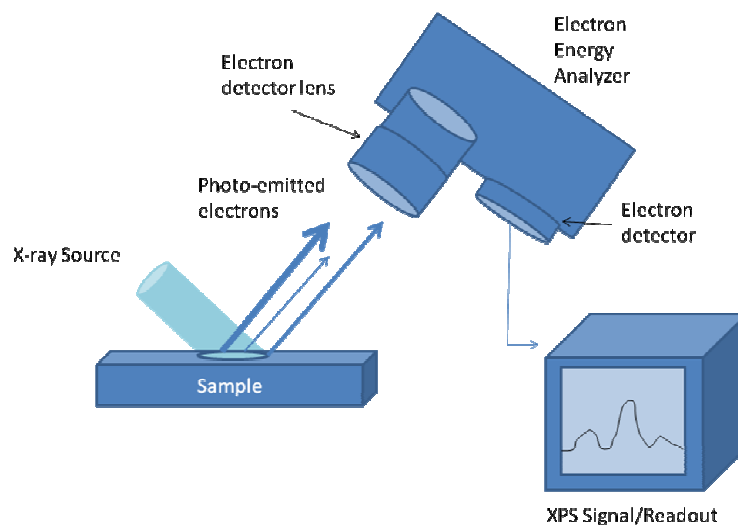


Figure 2.5 XPS Schematic

2.2.3 Experimental Preparation & Use

Precipitation identification in this work used FTIR, XPS, and SEM. FTIR analysis was performed for both the continuous-leak and single-leak experiments. Powdered samples of PbS were reacted for three days in both settings listed previously. Powdered sample were dried in the oven at 35°C to avoid any potential mineral phase changes due to higher temperatures, and then mixed with KBr powder (in a 1:20 ration of sample to KBr) and dried again. The sample was diluted 20 times for each sample and then analyzed with the FTIR after running a background sample. XPS samples were prepared by cleaving 5mm × 5mm galena samples and reacting with CO₂-H₂O salt solutions. After reaction, these samples were washed with DI water and then dried with high-purity nitrogen before undergoing XPS analysis.

2.3 Aqueous Chemistry

Aqueous chemistry is important information for understanding the reactions occurring in our system. Observations of heavy metal concentrations helps provide information to understand the dissolution processes and quantify the rate of dissolution. Flame-AA and ICP-MS were used to quantify concentration levels in this investigation.

2.3.1 ICP-MS – Principle

Inductively coupled plasma mass spectrometry is a commonly used tool for obtaining metal and several non-metal concentrations in the ppb and low ppm range. ICP-MS operates by using inductively-coupled plasma to ionize samples and then a mass spectrometer to separate, detect, and quantify ions. The sample solutions are introduced into the ICP-MS via a nebulizer and then ionized with Argon plasma before being analyzed with the mass spectrometer and sent to a computer for data analysis.

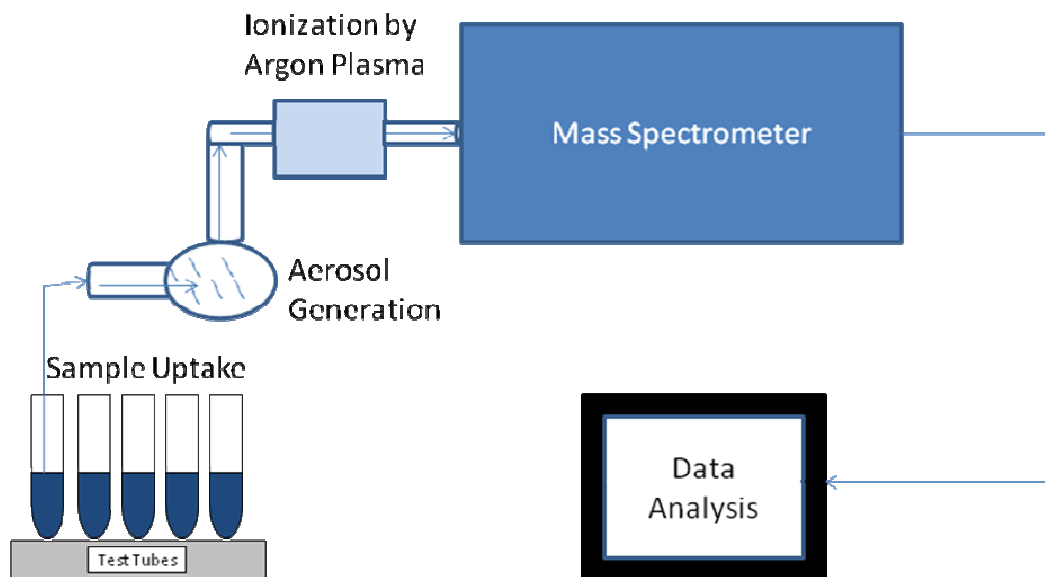


Figure 2.6 ICP-MS Schematic

2.3.2 Flame-AA Principle

Flame atomic absorption is another common technique for determining metal ion concentrations in aqueous environments. Based mainly on the Beer-Lambert Law, Flame-AA uses a flame to atomize the sample; the sample is mixed with combustible gases so the atoms of the element of interest is excited and absorb light at a specific wavelength. This energy is set by a specific wavelength and can be quantified and analyzed to obtain concentration measurements. Flame-AA is very effective measuring tool and has a detection range into the parts per million.

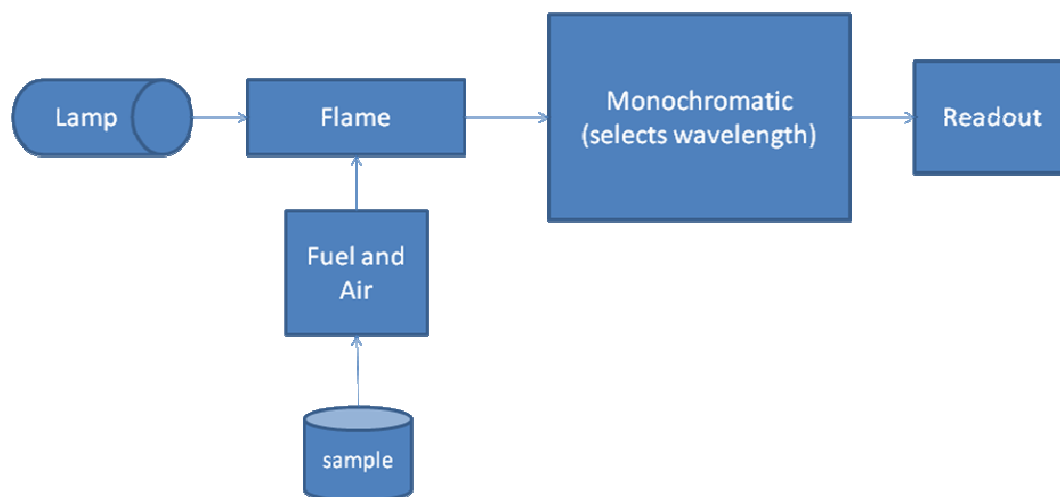


Figure 2.7 Flame-AA Schematic

2.3.3 Experimental Preparation & Use

Both ICP-MS and Flame-AA were used in the analysis of the experiments in this thesis. The Flame-AA was used to determine the lead concentrations for the powdered experiments since it was quick, easy and accurate. The instrument was calibrated with environmental standards and each standard were measured after seven measurements to ensure the validity of the curve. Each sample was diluted with a 0.5% HCl and 2% HNO₃ solution twice before being analyzed. The ICP-MS was used for analysis of the *in situ* AFM experiments since the Pb²⁺ concentrations were below the detection limit of the ICP-MS. Samples were prepared by diluting samples with 0.5% HCl and 2% HNO₃ solution; 1.0 M NaCl solutions were diluted 20 times solution while 0.01 M and 0 M solutions were diluted 3 times. All samples were then filtered with 0.2 μm filters to avoid introducing any solids into solution.

2.4 Surface Area

Surface area calculations were useful when normalizing data in the powdered galena experiment for dissolution rates and generally useful because the surface area in contact with solution is important in determining the dissolution rate. Geometric calculations were done for the galena samples in crystal form and the *in situ* AFM experiments while

BET measurements were conducted to obtain surface area values for the powdered samples.

2.4.1 BET – Theory & Use

BET is a method developed by Stephen Brunauer, Paul Huhg Emmett, and Edward Teller that is an extension of the Langmuir theory. BET utilizes adsorption of gas onto a solid surface to measure the specific surface area of a sample. The BET method used standard nitrogen gas and the typical 11-point analysis was performed. The BET value for the 1.0 g of powdered PbS (Alfa Aesar, 82% min) sample used was found to be 1.225 m²/g.

2.5 Experimental Design

The experimental design describes the three main experiments set up to investigate the dissolution and surface reactivity of galena through the various analytical tools described earlier.

2.5.1 *In Situ* AFM Experiment

Several *in situ* AFM experiments were conducted to investigate the dissolution of PbS and the effect of varying ionic strength. 0.0 M, 0.01 M, and 1.0 M NaCl solutions were prepared; unsaturated ($P_{\text{CO}_2}=0$) and saturated ($P_{\text{CO}_2}=1$) solutions tested for the effect of the introduction of CO₂. The pH of all unsaturated solutions was adjusted with HCl acid to equal the CO₂ saturated solution pH, where pH was approximately 3.78 ± 0.1 . Crystal samples of galena were cleaved along the (100) surface, with 1mm x 1mm x 1mm dimensions to ensure smooth operation of the fluid cell and mounted using dental wax. Solutions were pumped into the fluid cell at a rate of 0.5 mL per min and then passed through an in-line pH electrode before being collected at 5 minutes intervals for solution analysis.

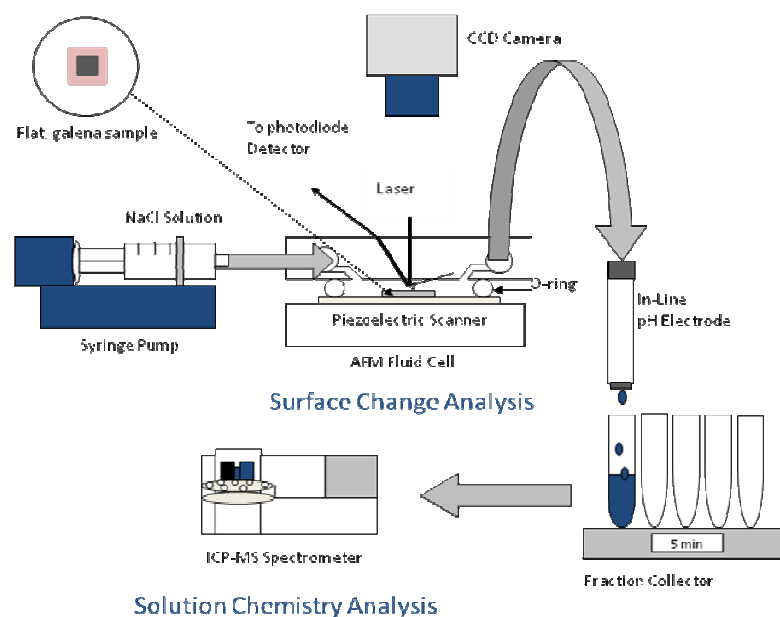


Figure 2.8 AFM *in situ* Experimental Setup

2.5.2 Single Leak Experiment

The single leak experiment was set up to model the scenario where CO_2 was released from the deep saline aquifer in one burst and the leak repaired quickly upon. To simulate this, a 1.0M NaCl, CO_2 saturated solution was reacted in 50 mL test tubes with 0.025g of PbS. Each simulation run was repeated to ensure enough samples were available for analysis and to provide better statistics. The pH was measured at the beginning and 3mL samples for Flame-AA analysis taken at given time intervals. Also, the solutions were filtered and the solid used for FTIR analysis. This same procedure was repeated with an unsaturated CO_2 solution by bubbling each salt solution with N_2 .

2.5.3 Continuous Leak Experiment

The continuous leak experiments sought to model the continuous release of CO_2 from deep, saline aquifers into ground level conditions. This was accomplished by bubbling CO_2 into 1 L of 1.0 M NaCl solutions, with 0.5 g of PbS, continuously and monitoring pH as well as collecting 3 mL samples for Flame-AA analysis. Measurements of pH and the IPC-MS sample were taken at 1, 3, 5, 10, 20, 30, 40, and 50 minutes, 1 hour, 2 hours, 3 hours, 5 hours, 1 day, 2 days, and 3 days. The solid PbS in the container was

then filtered and collected for FTIR analysis at the completion of the experiment. The same experiments were conducted with an unsaturated CO_2 solution to serve as a control.

Figure 2.9 shows a schematic of the single and continuous leak experiments, both conducted in a closed environment to ensure proper gas conditions were maintained.

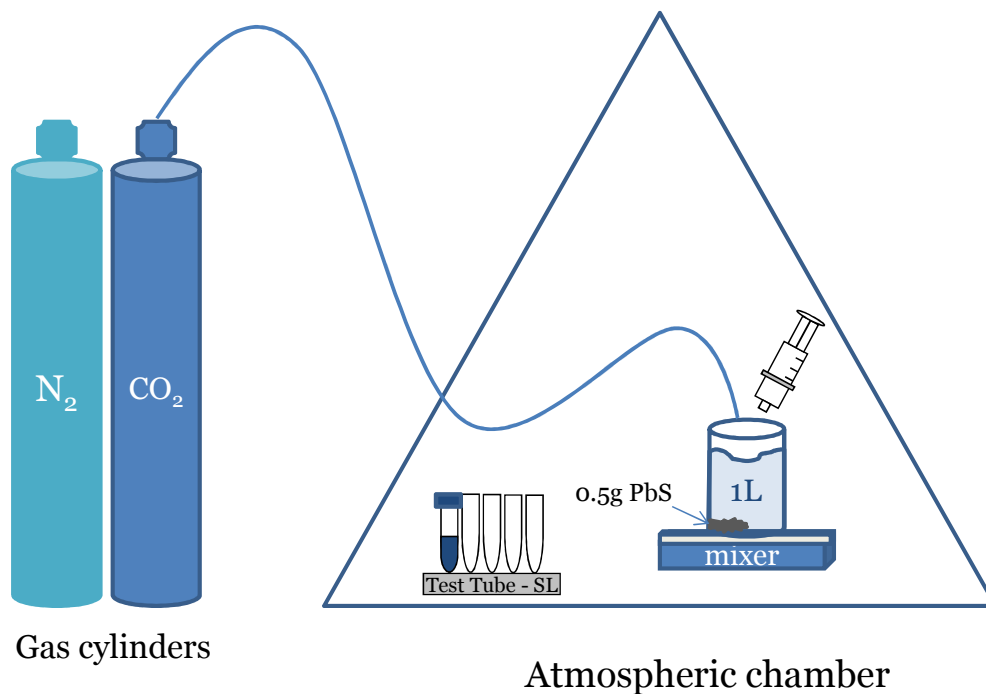


Figure 2.9 Experimental Schematic for Single & Continuous Leak Experiments

2.5.4 AFM *ex situ* Experiment

To investigate the reactions occurring on the surface of galena after interactions with CO_2 , an *ex situ* experiment was conducted. Utilizing atomic force microscopy the samples surface has been imaged. Samples were cleaved from galena and after looking through the microscope deemed either smooth or rough, which corresponds to either the (100) or (111)/(110) surface respectively. Nine samples were made and put into three separate test tubes: one for a sample with two smooth sides, one for a sample with two rough sides, and one for samples with one rough and one smooth side. The samples were reacted in two separate experiments with a CO_2 -saturated solution and a nitrogen-saturated solution for three hours. After reaction, the samples were rinsed

with DI water and then dried with high purity nitrogen gas before being examined under the AFM.

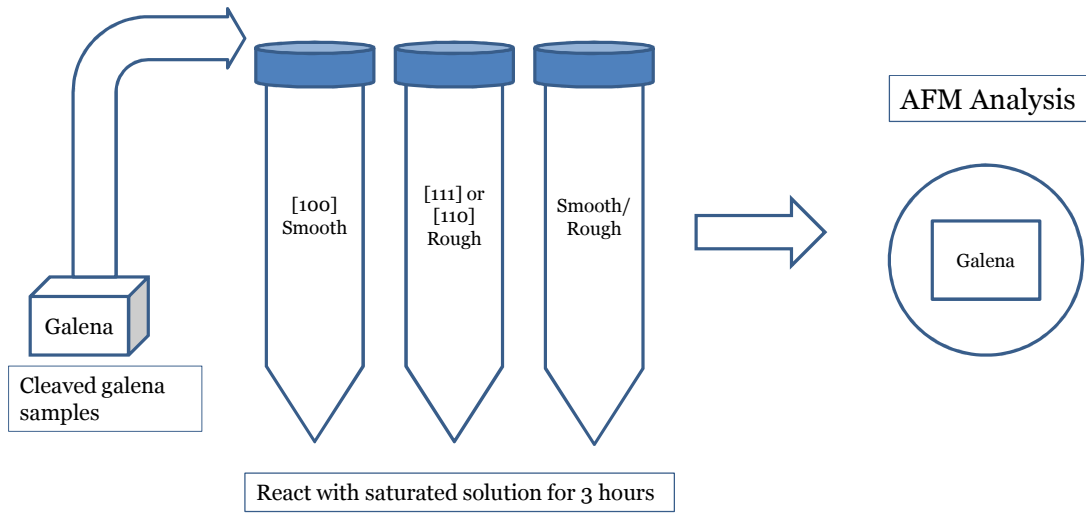


Figure 2.10 *Ex situ* AFM Schematic

Chapter 3

Results

This chapter describes the results obtained from the three main experimental designs detailed earlier. The concentrations and various spectra acquired through ICP-MS, Flame-AA, FTIR, and XPS are reported.

3.1 *In Situ* AFM Observations

The *in situ* AFM results provided critical information concerning the effect of varying the ionic strength of the solution and in quantifying the dissolution rate of galena at the specified conditions.

3.1.1 Aqueous Pb^{2+} Concentrations

The ICP-MS results for the six runs executed in the *in situ* set up are shown below. Trends for all the salt solutions and both the CO_2 saturated and unsaturated conditions are plotted below. The reported data shows very clear trends. The data shows an increased Pb^{2+} concentration in the unsaturated CO_2 condition as opposed to the CO_2 saturated condition as well as increased Pb^{2+} concentrations as the ionic strength of the solutions increases. The 1M NaCl condition saw a 24% increase in the Pb^{2+} concentrations in the unsaturated CO_2 condition compared to the saturated CO_2 solution going from around 90 ppb to 110 ppb. There was a 78% and 100% increase for the 0.01 M and 0 M NaCl cases respectively with concentrations changing from 27 ppb to 48 ppb for 0.01 M and 16 ppb and 32 ppb for the 0 M NaCl conditions. The data shows steady state conditions were met within an hour of injection.

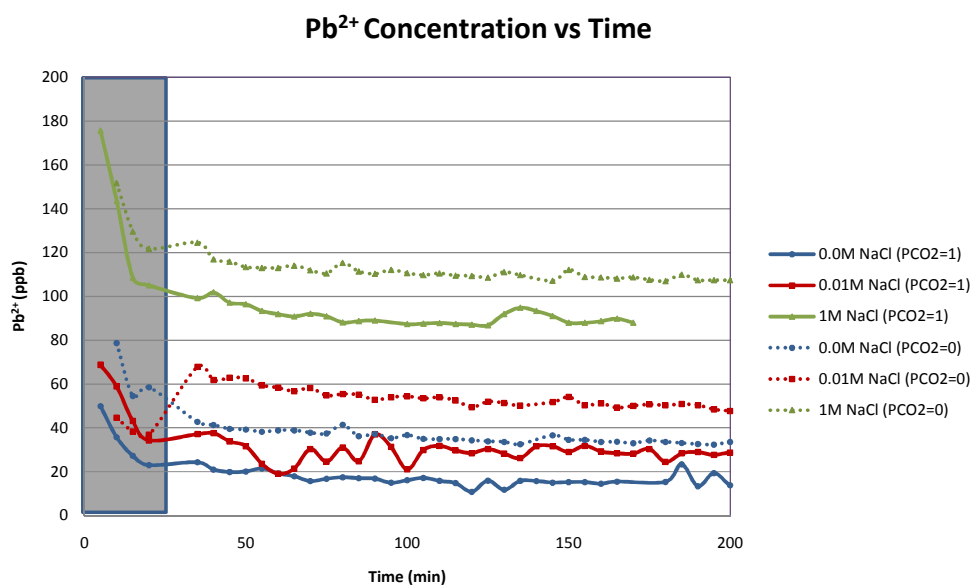


Figure 3.1 AFM *in situ* Concentration Results

3.1.2 Surface Morphology

Images from the *in situ* AFM experiment were not easily obtained during the fluid cell operation because of bubbles and focusing issues. Therefore, real time images of the changes on the surfaces are not available. The original surface of galena was imaged though at the beginning and the end of each run and noticeable changes were evident which were further investigated with the *ex situ* AFM experiments.

3.2 Single Leak Results

The single leak experiment was done to provide insight into the one-time, fixable leak from geological formations. Flame-AA and FTIR absorption analysis were conducted to understand the environmental impact of this scenario and quantify concentration rates and surface reactions.

3.2.1 Concentrations & FTIR Spectra

For the 1.0 M NaCl system, data comparing the saturated ($P_{CO_2}=1$) and unsaturated ($P_{CO_2}=0$) conditions is presented in Figure 3.2

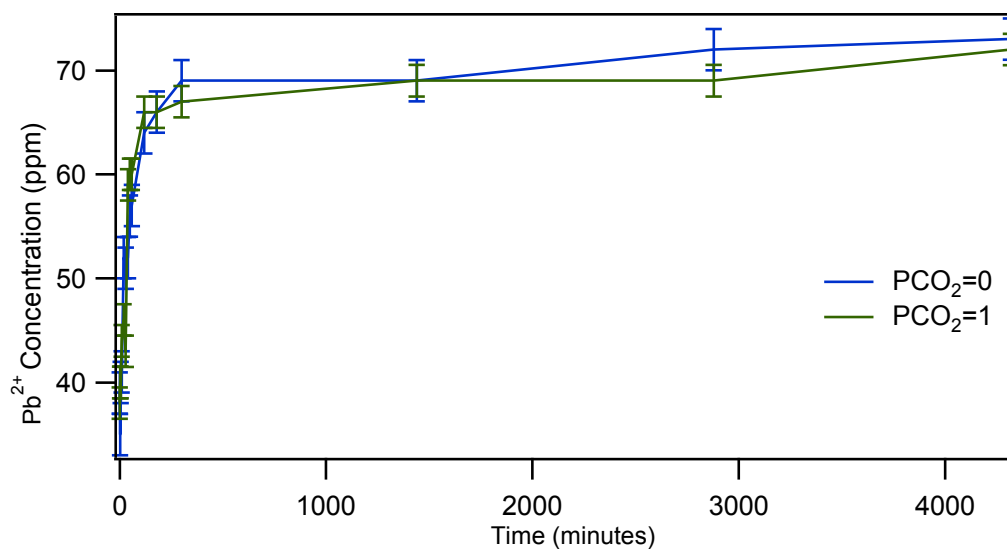


Figure 3.2 Single-leak: Pb²⁺ Concentration vs. Time:

Experiment run time: 3 days, pH=3.81, gas flow rate = 0.8 std. cubic feet per minute

The results for the single-leak experiment show very slight differences between the two systems, with the difference between the final data point being 1 ppm, which is a slightly less than 1.5% change between the two systems. While the graph is essentially the same, there still appears to be a trend where the unsaturated system is shown to have slightly higher concentration levels, particularly after the 5-hour data point, implying greater dissolution in the unsaturated scenario.

In order to fully understand the reactions occurring in the single-leak experiment for the 1.0 M NaCl system, FTIR data were collected from the end of the experiment (3 days). This sample was collected in a controlled environment (Captair system purged with the appropriate nitrogen or carbon dioxide gas) to reduce any potential reactions occurring from changing the experimental conditions.

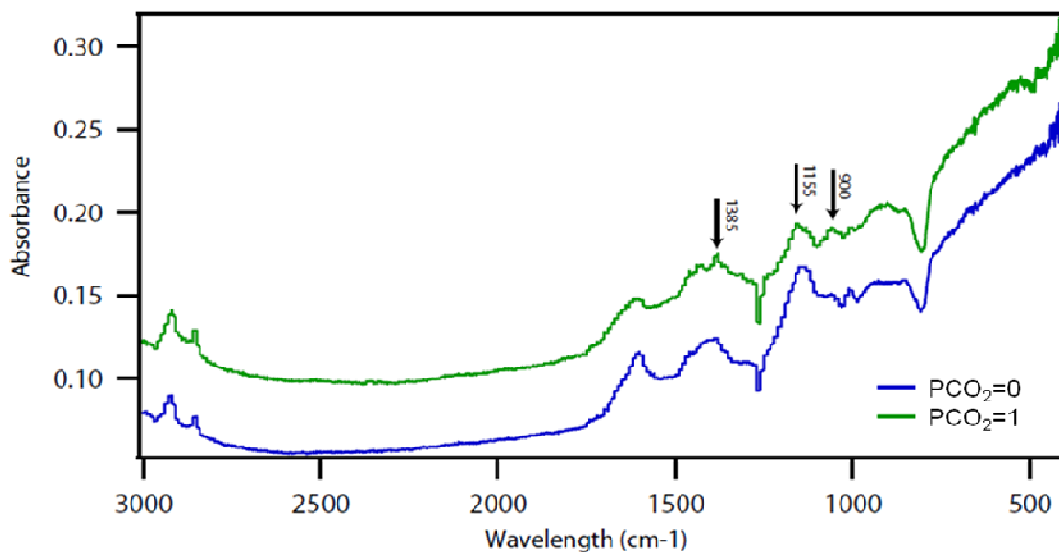


Figure 3.3 Single leak FTIR Absorption Spectra

Sample reacted 3 days, pH=3.81, gas flow rate = 0.8 std. cubic feet per minute

The FTIR data present in Figure 3.3 can be very helpful in identifying the mineral phases present in our sample. The top figure shows the general spectra for the sample while the bottom figure is an enlargement of the spectra from the 400 cm^{-1} to 800 cm^{-1} range. For the single-leak experiment significant changes in the spectra occur when comparing the saturated CO_2 and unsaturated CO_2 systems. The most significant differences occur, once again, the 500-700 cm^{-1} range. The development of peaks at 657 cm^{-1} and 526 cm^{-1} in the saturated CO_2 system are key differences between the two spectra. These peaks may correspond to a cystine, or S-S bond, signifying elemental sulfur on the surface or it could also be associated with lead carbonate. There is also a change in the spectra when comparing the peak in the 800 to 1200 cm^{-1} region. With the introduction of CO_2 , the peak around 1132 cm^{-1} is reduced and shifted to 1155 cm^{-1} , which is a peak associated with simply PbS. The broad plateau seen in around 850 cm^{-1} is raised and a peak develops around 900 cm^{-1} . Finally, there is also a noticeable change in the peak around 1385 cm^{-1} once the introduction of CO_2 occurs; the broad peak seen in the unsaturated system is sharper and stronger and a side peak at 1428 cm^{-1} has developed along with a small peak around 1310-1320 cm^{-1} which could be related to $\text{Pb}(\text{OH})_2$.

3.3 Continuous leak Results

The continuous leak experiment was done to provide insight into constant leakage of CO₂ from geological formations, perhaps through a natural fault or well fracture in the earth. Flame-AA and FTIR absorption analysis was conducted to understand the environmental impact of this scenario.

3.3.1 Concentrations & FTIR

The concentration data for the continuous leak experiment follows a similar trend to that seen in the single leak and *in situ* AFM experiments. The continuous leak experiment actually shows a more pronounced final concentrations change (64 ppm vs. 56 ppm, Figure 3.4) between the unsaturated and saturated conditions. The unsaturated condition has consistently higher Pb²⁺ levels from 2 hours onward for the duration of the experiment. The largest different between the two conditions occurs at the three hour mark, where the P_{CO₂}=0 solution, exhibits a 113% increase in Pb²⁺ concentration compared to the P_{CO₂}=1 scenario. By the end of experiment, the different between the two systems had stabilized, where the P_{CO₂}=0, Pb²⁺ concentrations were only about 14.5% higher than the P_{CO₂}=1 condition. This is interesting because CO₂ intrusion would be expected to have more Pb²⁺ release but the trend is otherwise, which may be explained by the consistent pH between both systems and the surface precipitations occurring in the CO₂-H₂O-PbS environment.

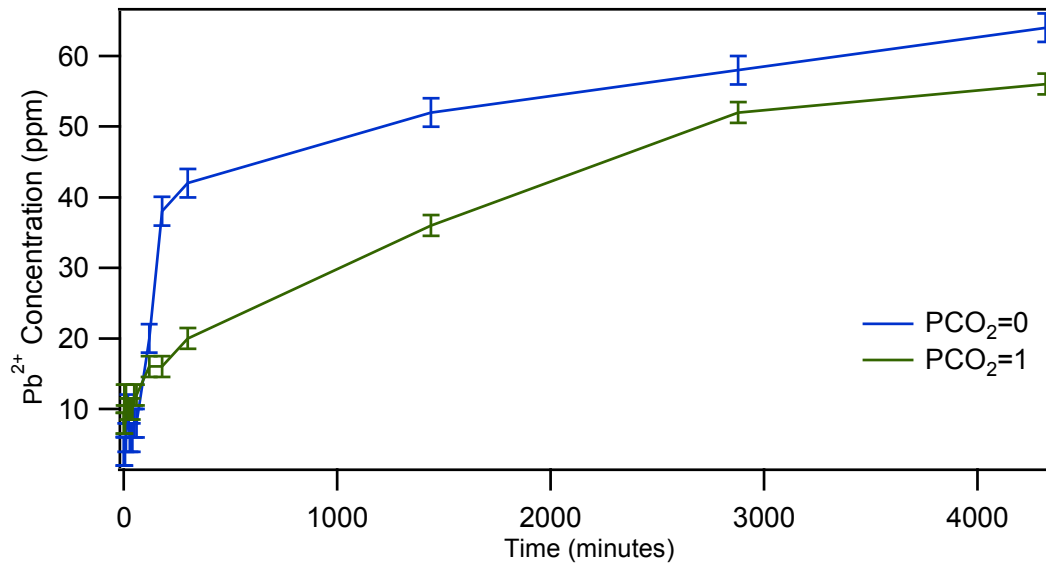


Figure 3.4 Continuous leak: Pb²⁺ Concentration vs. Time

Experiment run time: 3 days, pH=3.81, gas flow rate = 0.8 std. cubic feet per minute

FTIR analysis was also done for the continuous leak system, to help identify the mineral phases present for this reaction system. Figure 3.5 shows the FTIR absorption spectra for both the unsaturated and saturated CO₂ conditions.

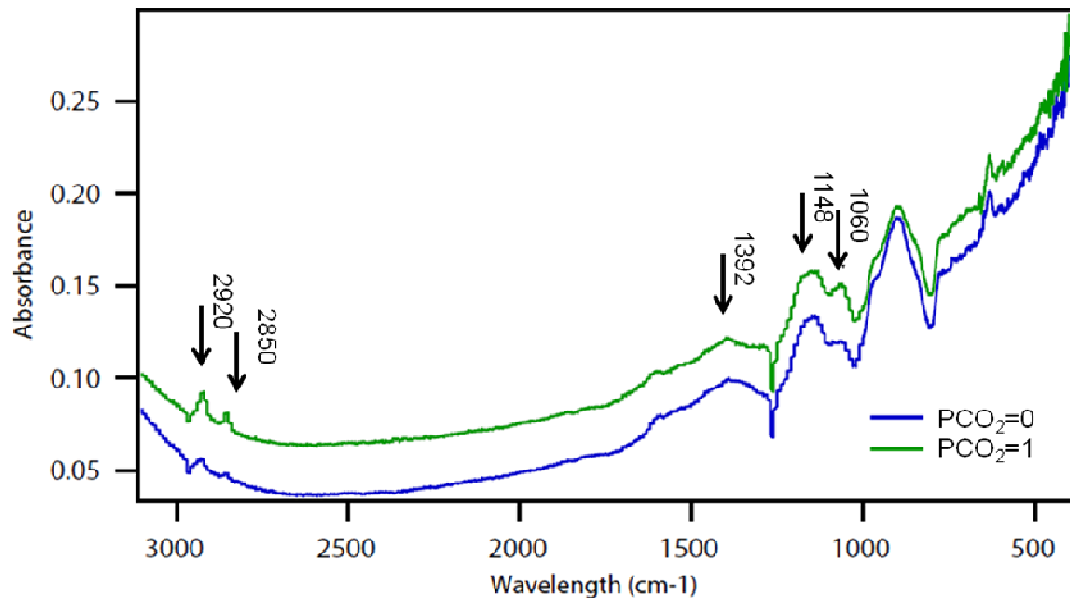


Figure 3.5 Continuous leak FTIR Absorption Spectra

Experiment run time: 3 days, pH=3.81, gas flow rate = 0.8 std. cubic feet per minute

The FTIR data collected for both the single-leak and continuous leak experiment can help in analyzing the surface species found on galena. Again, the top image in Figure 3.5 is the overall FTIR spectra while the bottom image is an enlargement of the region between 500 cm^{-1} and 700 cm^{-1} . To begin with the continuous leak scenario, the greatest changes in the spectrum occur in the $550\text{-}700\text{ cm}^{-1}$ range; the introduction of CO_2 into the experimental system shows the formation of a new peak at 661 cm^{-1} and stronger, pointed peaks at 630 cm^{-1} and 590 cm^{-1} which may correspond to PbSO_4 . There are a few other changes occurring in the spectra. With the introduction of CO_2 , a stronger peak develops at 1060 cm^{-1} , which could correspond to PbCO_3 while the peak at 1148 cm^{-1} which is closely aligned with just PbS broadens out slightly. The peak at 1392 cm^{-1} , also corresponds to PbOH of PbSO_4 , and changes as CO_2 enters the system, flattening out a bit, making the peak more pronounced. While less useful in identifying the mineral species present on the surface, the CO_2 saturated system shows sharper peaks at 2920 cm^{-1} and 2850 cm^{-1} which corresponds to C-C aliphatic bonding.

While this data is useful, there are several drawbacks to using the FTIR for peak identification in this system. First, the amount of secondary mineral formation compared to the bulk mineral sampled is very small making the changes in the peak very small and difficult to distinguish sometimes. Secondly, many references noted certain ranges of wavelength values corresponding to certain mineral phases resulting in some uncertainty to the accuracy of each peak match. The benefit of FTIR is seeing noticeable changes in the spectra when comparing different conditions. For both the single and continuous leak systems, there are significant changes in the system when the solutions contained CO_2 or not. This change motivates further studies and prompts the use of other techniques to corroborate and help clearly identify the secondary mineral precipitations. Again, the FTIR data is useful when you compare the changes seen in the single and continuous leak experiments. These differences can be assigned to different compounds to help begin to unravel what is the reaction occurring and how as well as to what extent the $\text{PbS-H}_2\text{O-CO}_2$ system is changing in different conditions.

Continuous and Single Leak Comparison

The results of the FTIR analysis for both the single-leak and continuous-leak experiment show that some significant change is occurring in each system with the introduction of CO₂. Even more insight into the reactions occurring in these environments can be gleaned when comparing the differences found between the single-leak and continuous-leak experiments.

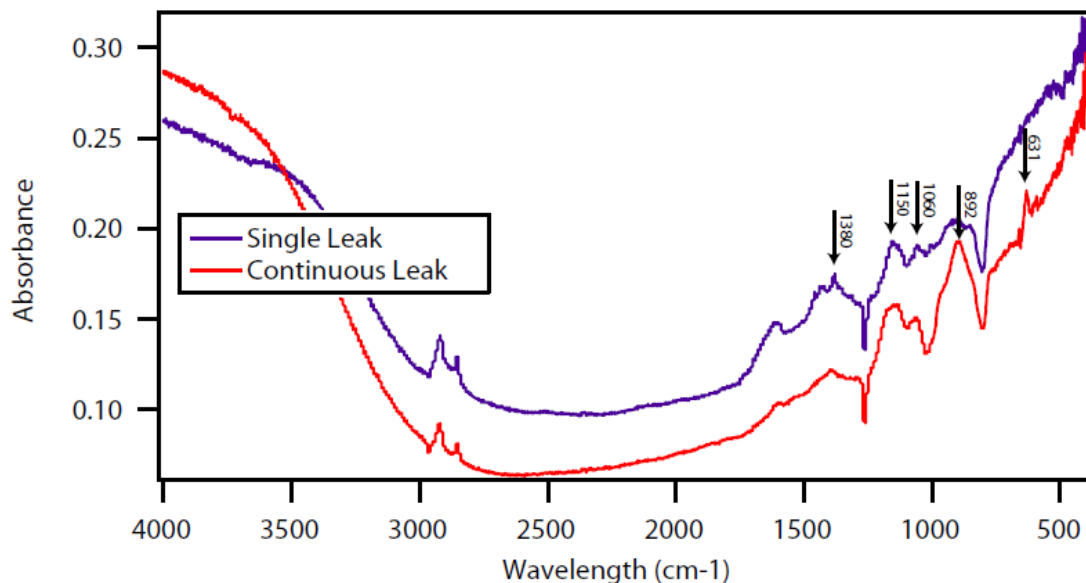


Figure 3.6 FTIR Absorption Spectra: CO₂ Saturated Conditions:
Comparison between continuous and single leak experiments.

There are also some noticeable changes when the single-leak experiments are compared with the continuous leak scenarios. For the single-leak and continuous leak experiments, in the CO₂ saturated environment, FTIR peaks at 2929 cm⁻¹, 2854 cm⁻¹, and 1600 cm⁻¹ stay relatively consistent. However, noticeable changes occur in the continuous leak experiment with the development of a strong, intense peak found at 892 cm⁻¹ and the disappearance of the 900 cm⁻¹ peak seen in the single-leak experiment. Alterations in the peaks at 1380 cm⁻¹, 1150 cm⁻¹, and 1060 cm⁻¹, which can correspond to PbOH or PbSO₄, change as these peaks are sharper and more distinct in the single-leak experiment. The continuous peak shows lesser intensity peaks at the same values in the single leak, 1380 cm⁻¹, 1150 cm⁻¹, and 1060 cm⁻¹. There is also a strong peak development at 631 cm⁻¹ which corresponds to PbSO₄.

3.4 *Ex Situ* AFM Observations

Ex situ AFM experiments were conducted to examine the surface morphology changes on the surface of galena after reactions with CO₂. Samples were imaged with both contact and tapping modes, with the majority of quality images using tapping mode. Height and width dimensions were obtained as well as surface coverage of precipitation calculated.

3.4.1 Unsaturated CO₂ Condition (P_{CO₂}=0)

The unsaturated CO₂ solution serves as the control case for our system to observe what the impact of the CO₂ to the system is. A typical image of the unsaturated CO₂ solution is shown below in figure 3.7

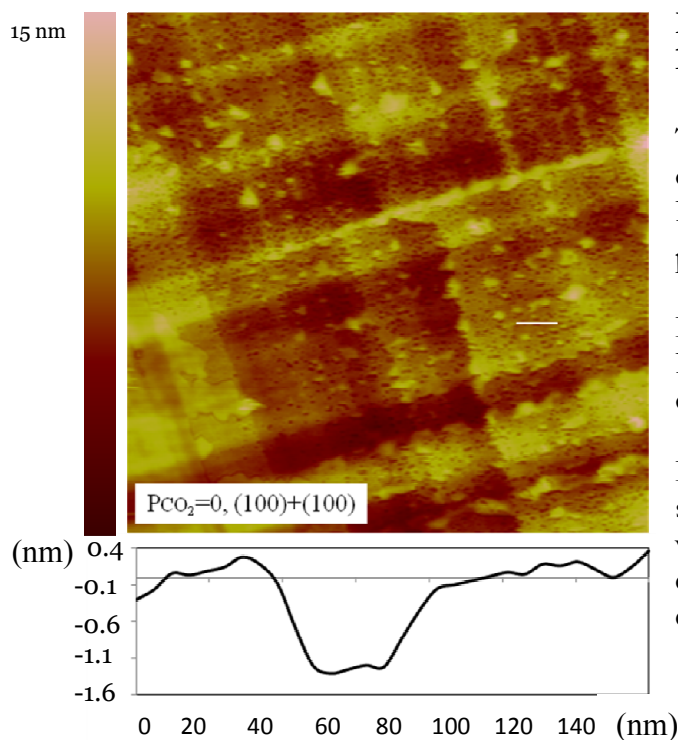


Figure 3.7 AFM Image of Dissolution, P_{CO₂}=0

Tapping mode AFM image of dissolution pit in 1.0 M, P_{CO₂}=0, NaCl solution with pH=3.78.

Image of (100) surface of PbS sample with both slides cleaved along (100) planes.

Image is 2.5 μm wide. Data scale is 15 nm. Height vs. width data for specific dissolution pit is 1.14 nm deep and 33.3 nm wide.

The main features of the P_{CO₂}=0 system are dissolution pits. While some precipitations were also found on the surface of the unsaturated samples, dissolution was the dominant mechanism and the most commonly observed feature. The samples imaged were cleaved and imaged along the (100) surface to obtain the dimensions of

each pit. The average depth of the dissolution pits found on the surface of the samples was 1.30 nm and the average width of these pits is 39.5 nm based on an average of dimensions from 15 sample dissolution pits.

3.4.2 Different Planes – (100) and (110)/(111)

The reactivity of different planes of galena was investigated by cleaving specific planes on each sample. Samples were prepared with each side cleaved along different planes as described previously; images and quantification of precipitation was based off the (100) plane.

The first system investigated has each side of the PbS sample cleaved along the natural cleavage (100) plane of galena. Figure 3.8 below is a representative image of the reaction of PbS-H₂O-CO₂ and shows the development of precipitation on the surface.

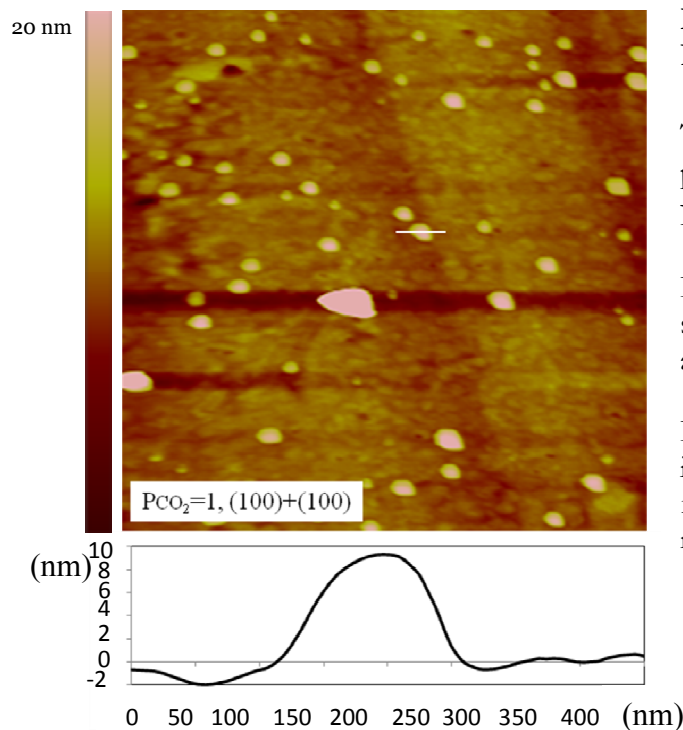


Figure 3.8 AFM Image of Precipitation (100), P_{CO₂}=1

Tapping mode AFM image of precipitation in 1.0 M, P_{CO₂}=1, NaCl solution with pH=3.78.

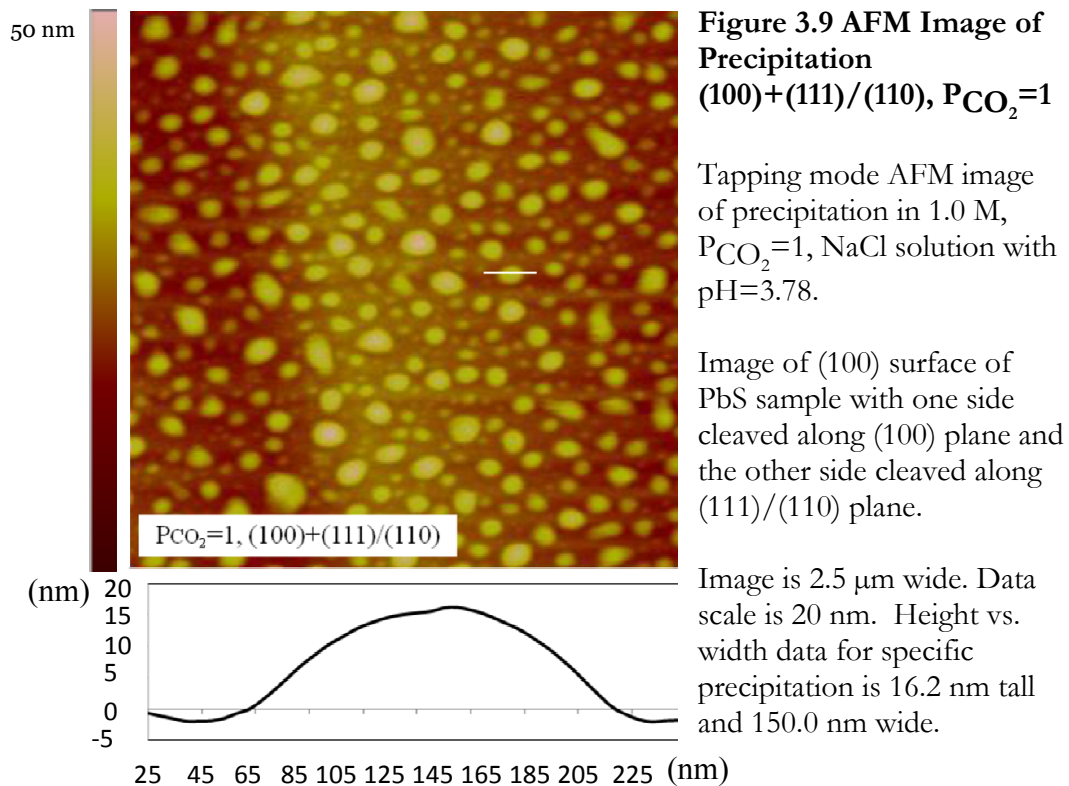
Image of (100) surface of PbS sample with both slides cleaved along (100) planes.

Image is 3.0 μm wide. Data scale is 20 nm. Height vs. width data for specific precipitation is 9.8 nm tall and 139.0 nm wide.

The image shows the development of clear, uniformly shaped precipitate on the surface of galena. The circular shape of the precipitations implies an amorphous secondary mineral phase because it lacks the clear, strong lines of a crystalline structure. The average height for the precipitations found on this surface in the CO₂ saturated

condition is 8.55 nm and the average width is 145 nm based on an averaging of height and width dimensions for seventeen separate precipitations. The frequency of these precipitations occurring is between 3.6% and 4.6% of the entire area imaged, calculated by finding the area covered by every clear precipitation on the surface (50 analyzed) and determining the ratio of this area to the total area available on the surface.

The second system analyzed were samples that were cleaved with one side along the (100) surface and the other side along the (110)/(111) surface. Figure 3.9 is a representative image of the reaction between PbS-CO₂-H₂O and shows the development of precipitation on the (100) surface in this setting.



The image shows clear precipitation on the surface; again the spherical shape of the secondary mineral phase implies a meta-stable species. The precipitations are fairly uniform and dispersed throughout the surface. The average height of precipitations found on this surface is 12.08 nm with the average width being 126 nm. These numbers were based off dimensions measurements thirteen specific precipitations – 7 for the larger particles present on the surface and 6 for the smaller particles. These

numbers were then weighted for the fraction of the surface covered with smaller particles compared to larger particles (3/4 to 1/4 respectively). For these samples, the frequency of precipitations was much greater, doubling the rate of occurrence. Precipitation on these surfaces covered approximately 24.0% of the surface area based off area calculations of 80 precipitations.

A summary of the quantitative data obtained from the *ex situ* AFM images is found in Table 3.1. The precipitations were moderately larger in the second setting with one smooth and one rough cleavage and the surface coverage increased nearly 20% when one side was roughly cleaved.

Table 3.1 Secondary Mineral Precipitation Analysis

Precipitations		
	(100)	(111)+(110)
Average Height	8.5 nm	12.01 nm
Average Width	145 nm	126 nm
Surface Coverage	4%	24%

3.4.3 Cleavage Planes: (111) & (111)/(110) Surface

While cleavage of galena along the (100) can be easily prepared, preparation of PbS samples along the (111) or (111)/(110) plane is more difficult. The (111)/(110) cleavage was obtained after several attempts to cleave the sample poorly to ensure a rough edge. Figure 3.10 is a representative image of the surface exposed during the *ex situ* experiments.

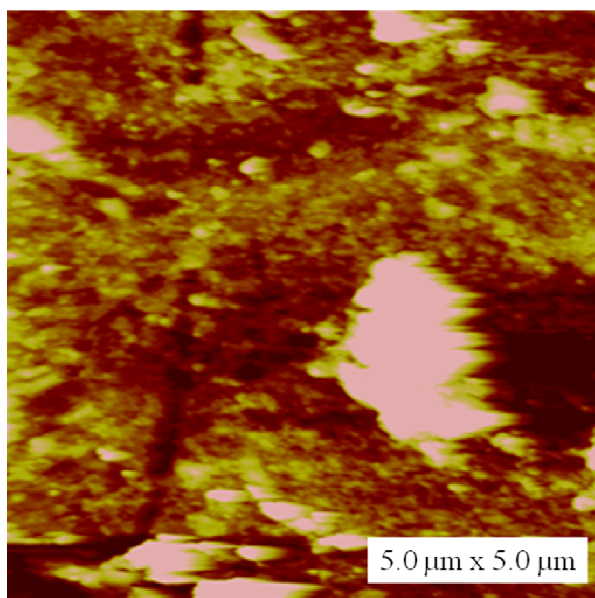


Figure 3.10 AFM Image of Rough (111)/(110) Surface:
Tapping Mode, 1.0 M, $P_{CO_2}=1$, NaCl solution with pH=3.78. Data scale 50 nm.

The image highlights the extreme variations in height on the (111)/(110) cleaved surface, which hindered the opportunities to obtain quality images. Evidence of dissolution are evident in images of this surface.

In order to image the (111) plane exactly, PbS samples must be sent to Princeton Scientific Inc. (NJ) to be specially cut and polished along (111) plane. These samples can then be reacted and imaged with the AFM. The figure below is a typical image of the (111) surface after reaction with $PbS-CO_2-H_2O$. The (111) image carefully prepared also shows evidence of dissolution on the surface as well as some limited precipitation.

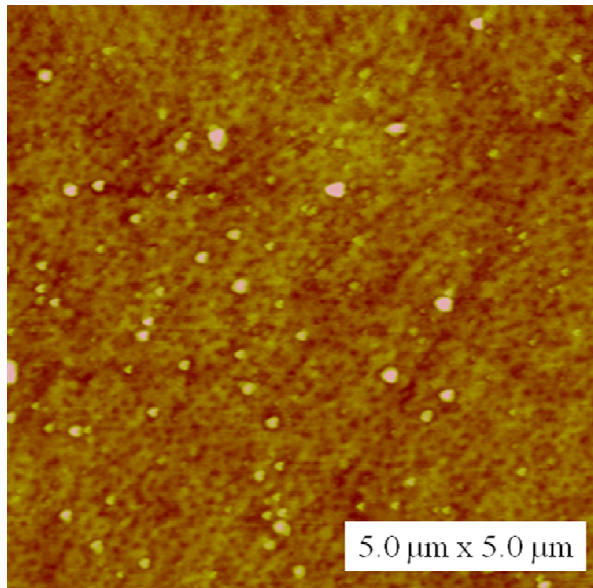


Figure 3.11 AFM Image of (111) Surface
Tapping Mode, 1.0 M, $P_{\text{CO}_2}=1$, NaCl solution with $\text{pH}=3.79$. Data scale 15 nm.

3.5 SEM Results

Both crystal and powdered samples of galena were imaged after reaction with CO_2 -salt solutions for three days. Crystal samples were imaged of the (100) plane.

3.5.1 Single Crystal Samples

Images of galena samples with both sides cleaved along the (100) plane were taken in 1.0 M NaCl solutions in saturated and unsaturated CO_2 conditions.

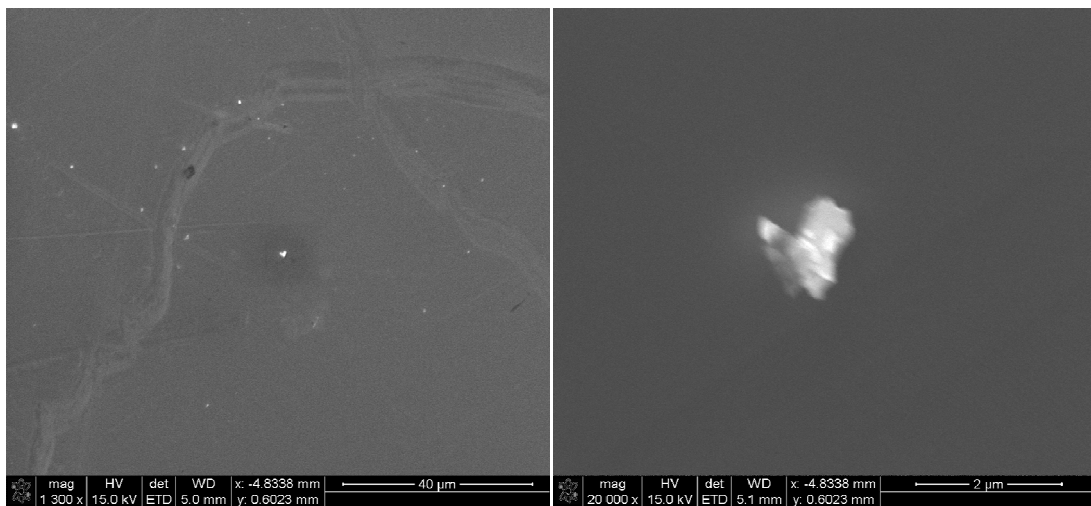


Figure 3.12 SEM Image: (100) Surface, $P_{\text{CO}_2}=0$. Analysis on sample reacted for 3 days in 1.0 M NaCl solution at pH=3.8

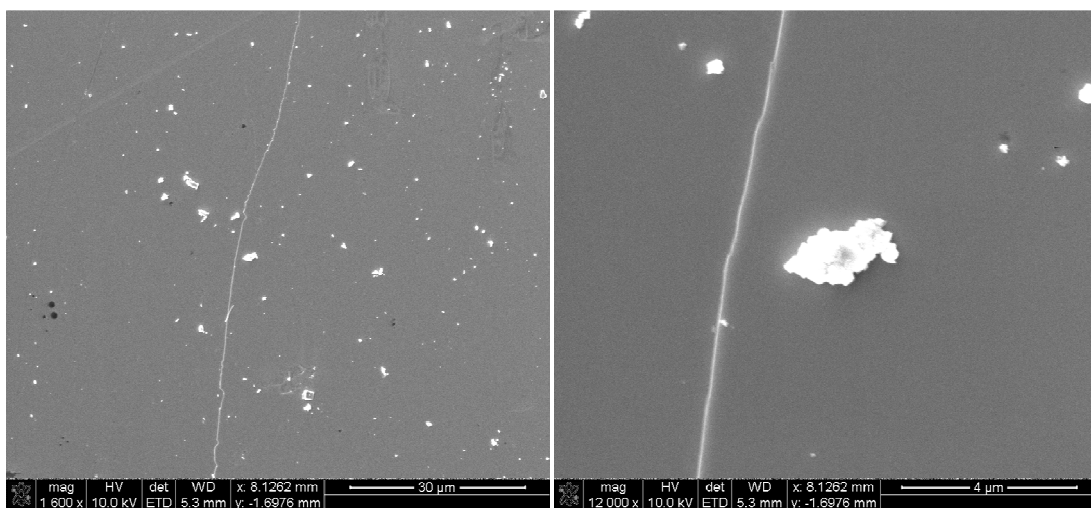


Figure 3.13 SEM Image: (100) Surface $P_{\text{CO}_2}=1$. Analysis on sample reacted for 3 days in 1.0 M NaCl solution at pH=3.80.

The collected images for the crystal surface confirm the trend observed in the AFM results. There is more precipitation occurring on the surface reacted at $P_{\text{CO}_2}=1$ (see Figure 3.13). The shape of these formations is not clear though it does appear in the image to the right in Figure 3.13 that aggregations of species may be occurring.

3.5.2 Powder Samples

The powder samples of galena imaged come from the continuous leak experiments that reacted for three days in a CO₂ saturated and unsaturated environment.

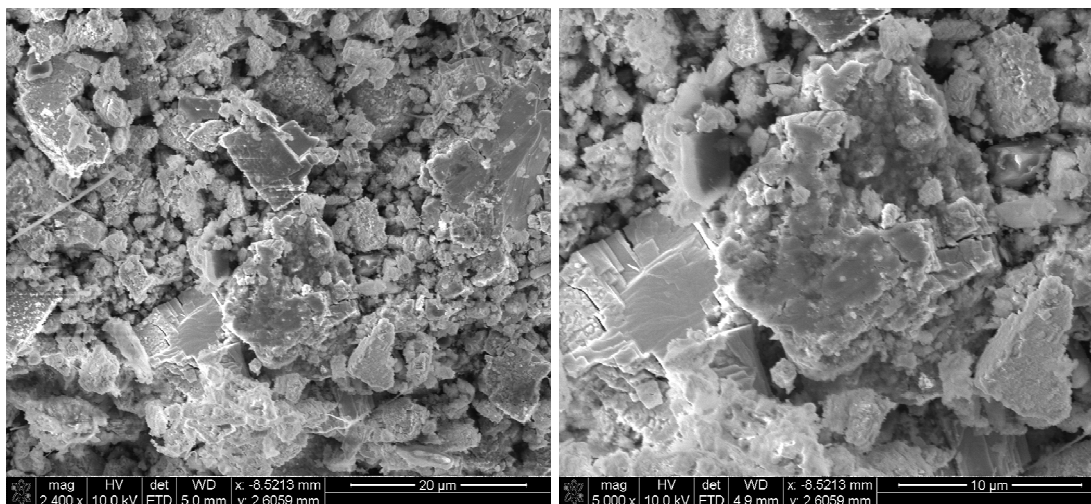


Figure 3.14 SEM Image: Powder Surface, $P_{\text{CO}_2}=0$ - Analysis on sample reacted for 3 days in 1.0 M NaCl solution at pH=3.80.

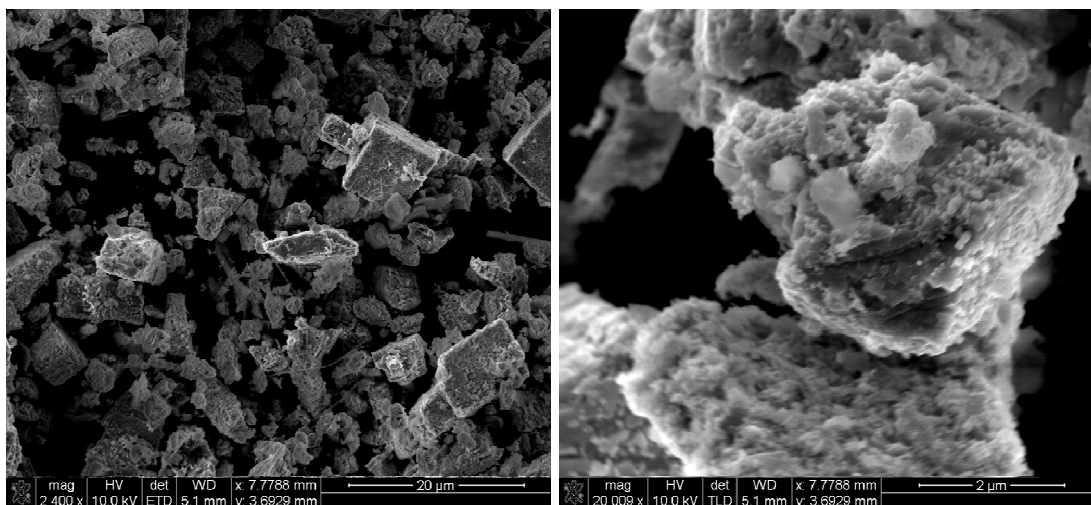


Figure 3.15a SEM Image: Powder Surface, $P_{\text{CO}_2}=1$ - Analysis on sample reacted for 3 days in 1.0 M NaCl solution at pH=3.80.

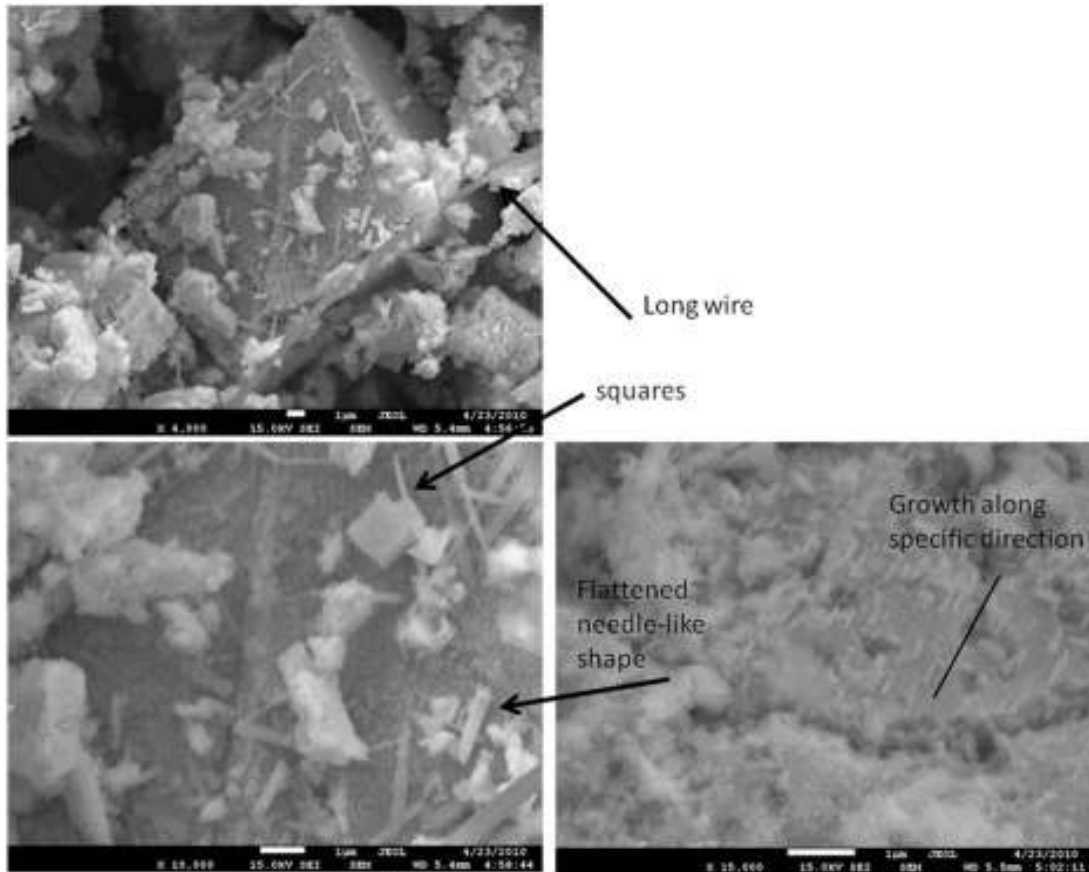


Figure 3.15b SEM Image: Powder Surface, $P_{\text{CO}_2}=1$ - Analysis on sample reacted for 3 days in 1.0 M NaCl solution at pH=3.80.

The powder SEM images also provide some information on the surface morphology. In the $P_{\text{CO}_2}=0$ system, there is not a lot of precipitation present on the surface and no clear pattern of shapes are formed. In the $P_{\text{CO}_2}=1$ system, there is evidence of more growth on the sample surface. There is also a more established pattern of shapes observed with the formation of square and flat, almost needle-like precipitations on which appear to demonstrate oriented growth on the crystal surface. There is also evidence of a long, thin wire apparent after reaction with CO_2 .

3.6 XPS Results

XPS results were performed on 5 mm x 5 mm galena samples cleaved along the (100) plane and prepared exactly the same as the *ex situ* experiment for both the CO_2

saturated and unsaturated environments. This data yielded some very interesting results about the composition of the surface on galena.

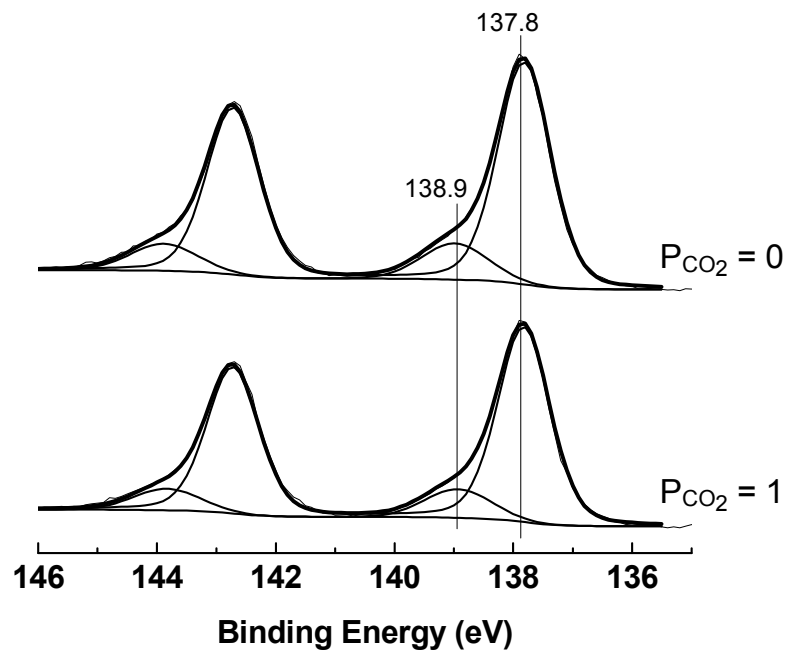


Figure 3.16 XPS Results – Pb 4f Spectra: $PCO_2=0$ (Top) and $PCO_2=1$ (Bottom)
Analysis on (100) cleavage reacted for 3 days in 1.0 M NaCl solutions at pH=3.80.

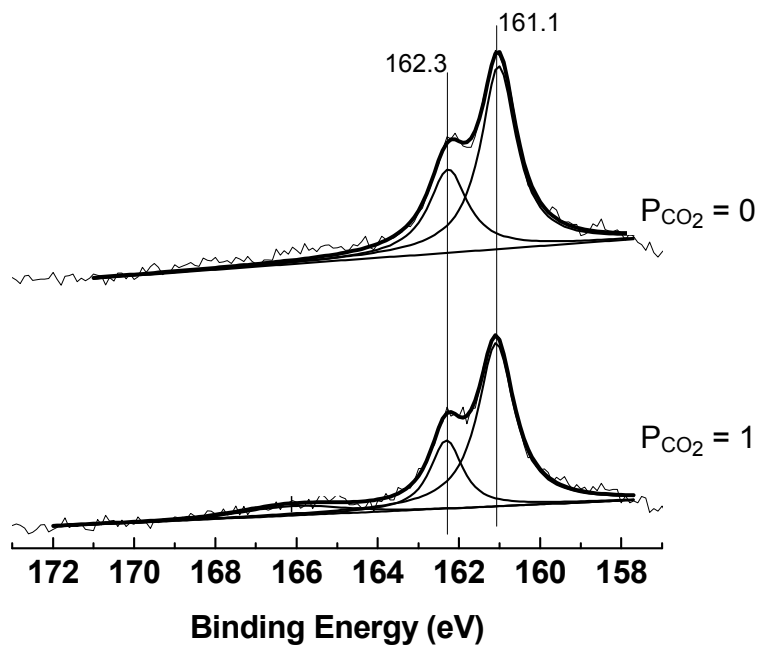


Figure 3.17 XPS Results – S 2p Spectra:
 $PCO_2=0$ (Top) and $PCO_2=1$ (Bottom) Analysis on (100) cleavage reacted for 3 days in 1.0 M NaCl solutions at pH=3.80.

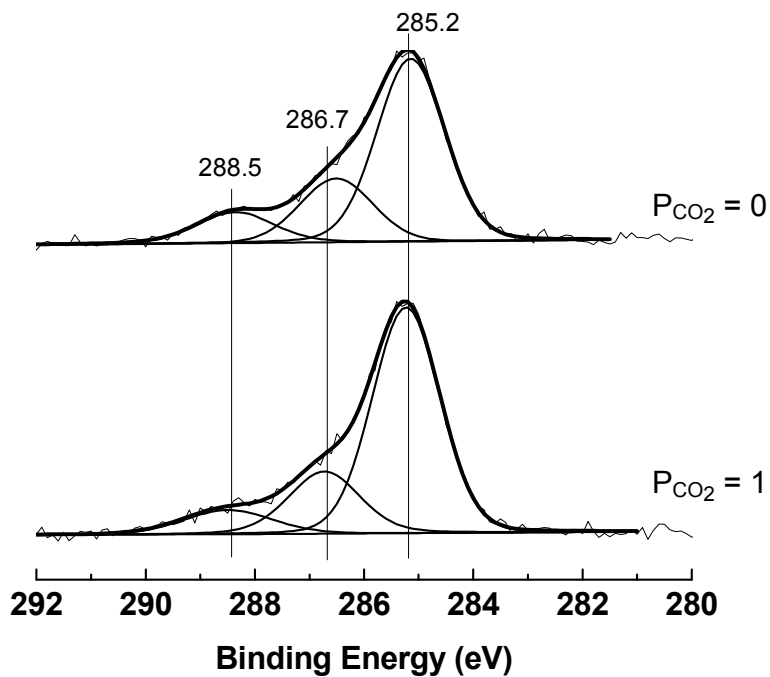


Figure 3.18 XPS Results – C 1s Spectra:
 $PCO_2=0$ (Top) and $PCO_2=1$ (Bottom) Analysis on (100) cleavage reacted for 3 days in 1.0 M NaCl solutions at pH=3.80.

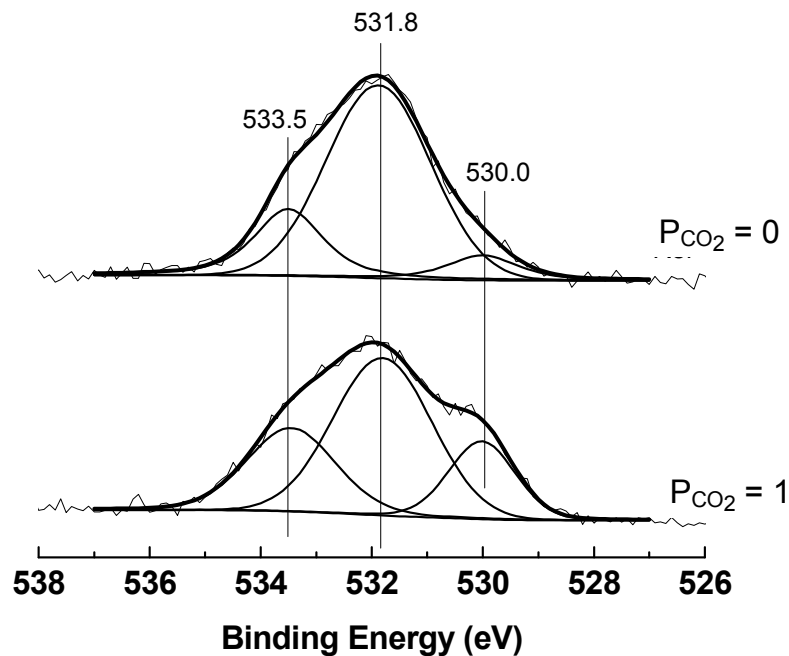


Figure 3.19 XPS Results – O 1s Spectra:

PCO₂=0 (Top) and PCO₂=1 (Bottom) Analysis on (100) cleavage reacted for 3 days in 1.0 M NaCl solutions at pH=3.80.

The XPS results for lead, sulfur, carbon, and oxygen are shown above; detailed spectra are shown after background subtraction and curve synthesis. Peak assignments were made for each element. For lead, two peaks, Pb4f_{7/2} and Pb4f_{5/2}, are observed from contributions due to spin-orbiting splitting. The binding energies of 137.8 eV and 138.9 eV can be assigned to PbS and PbSO₃, PbCO₃ or PbO [40-42]. Sulfur exhibits binding energies at 161.1 eV and 162.3 eV correspond to PbS. Around 166.1 eV (corresponding to PbSO₃), there is some signal, but it can be due to surface roughness [42, 43]. For the carbon spectra, binding energies are evident at 285.5 eV, 286.7 eV, and 288.5 eV which are associated with aliphatic, C-C, bonding, C-O bonding, and PbCO₃ respectively [35, 44, 45]. Finally, the oxygen spectra the binding energies at 530.0 eV, 531.8 eV, and 533.5 eV can be assigned to PbO, PbSO₃ or PbCO₃, and Pb(OH)₂ respectively [35, 40, 46].

The sample reacted in the PCO₂=0 or nitrogen saturated environment acted as a control for this experiment to see the influence of CO₂. The PCO₂=0 system is shown in the top spectra above for each element, while the PCO₂=1 spectra is shown on the bottom.

The XPS spectra proved very interesting in assessing CO₂ impact and providing information as to what may be forming on the surface of galena. The spectra for Pb 4f and S 2p stayed fairly consistent from one experimental condition while the C 1s and O 1s displayed some clear variations with the introduction of CO₂. The carbon spectrum saw changes at the 285.5 and 288.5 energy levels with the peak at 288.5 eV decreasing slightly and the peak at 285.5 eV becoming stronger. The oxygen spectrum also saw distinct changes with a slight decrease at 531.8 eV and slight increase at 533.5 eV. A significant increase in the intensity of the peak at 530.0 eV also occurred. Another interesting result from this analysis was the strong presence of carbon and carbonate species in the nitrogen reacted system, implying the introduction of oxygen somehow (perhaps via the nitrogen gas used) or an effect of cleaving samples in the area signaling perhaps a need for greater cleaning of the surface before reaction.

Chapter 4

Discussion

The results displayed in Chapter 3 provide much data for understanding the interactions between PbS-CO₂-H₂O and the surface reactivity of galena. In this chapter, the mechanisms and explanations for these results will be explained.

4.1 Effects of Aqueous Chemistry & Ionic Strength

The aqueous chemistry analysis in the solutions for the various experiments conducted provides much insight into the interactions occurring in our system and allows for a quantification of the release of Pb²⁺ from galena into solution. From the *in situ* AFM experiments, single leak and continuous leak experiments (Figure 3.1), the Pb²⁺ concentrations at various salt concentrations were obtained and a general trend apparent when comparing the saturated CO₂ and unsaturated CO₂ solutions. The unsaturated CO₂ solution at the same pH reveals higher Pb²⁺ concentrations for each of the three experiments attempted. This data is unexpected, because the introduction of CO₂ was assumed to continue to lower the pH, which would result in higher metal dissolution. Instead, pH measurements stayed relatively steady and the unsaturated condition is shown to have more Pb²⁺ in solution as there is greater dissolution and reprecipitation in the with CO₂ case. The difference in the concentration levels for the PCO₂=1 and PCO₂=0 conditions can be explained by the potential reactions occurring in each environment. This data indicated increased precipitation or re-precipitation in the saturated CO₂ system as the formation of secondary minerals would react and keep Pb²⁺ ions from being released into the water. Since the unsaturated system has higher levels of Pb²⁺ in the aqueous phase, the dissolution process is more permanent as the Pb²⁺

ions released are not re-precipitating on the surface to the same degree in the saturated system.

The other evident trend from the concentration data obtained showed the effect of ionic strength. The 1.0 M NaCl solution was shown to have much higher Pb^{2+} concentrations in solution than the 0.01 M or 0 M solutions. The higher salt concentrations means that activity must be accounted for when calculating concentrations; high salt concentration results in a lower activity since the ions in solution are not moving as much. Lower solution activity would result in an actual concentration less than the equilibrium concentration.

$$\sigma = \ln\left(\frac{AP}{K}\right) \quad (1)$$

If the AP value is lower than the equilibrium, K, than the saturation index would be less than one. Generally, if the saturation index is less than one, then precipitation is less likely to form. This rationale also helps explain why Pb^{2+} concentrations would be higher for the 1.0 M NaCl system.

The concentration levels of Pb^{2+} obtained from the single-leak and continuous-leak experiments also provide some insight into the dynamics of the PbS- H_2O - CO_2 system. There is a more significant difference between the Pb^{2+} concentration levels for the $\text{P}_{\text{CO}_2}=1$ and $\text{P}_{\text{CO}_2}=0$ scenarios in the continuous leak experiment than in the single leak experiment. This result may be explained by the reactions occurring in the presence of CO_2 . While the single-leak experiment exposes PbS sample to CO_2 , this occurs at one time only and perhaps the level of CO_2 in the solution dissipates slightly as CO_2 may escape the test tube holder. Because there is only one opportunity for CO_2 to enter the system and there is the potential this CO_2 escapes slightly, the reaction occurring is more similar to the unsaturated solution case, hence the little difference in concentration levels. For the continuous system, the concentration level difference is more pronounced because a steady flow of CO_2 is directed into the system, allowing for the reactions to continue and the formation of precipitations on the surface to develop. This would explain why the continuous leak sees a greater difference in the

concentration levels of Pb^{2+} for the saturated and unsaturated systems than the single-leak experiment.

4.2 Dissolution and Precipitation Rates

This work sought to obtain the experimental dissolution and precipitation rate for galena to provide information on the kinetics of the reaction occurring.

Dissolution Rates The dissolution rate is valuable information for determining the impact of CO_2 leakage on the groundwater quality as it provides a measure of the Pb^{2+} concentration that will be found in solution. The dissolution rate for galena was easily quantified in the *in situ* AFM experiment since the experiment was structured as a simple flow-thru experiment without any lead present in the solution initially and it reached equilibrium conditions. The dissolution rate of galena was calculated by:

$$R_{pb} = Pb^{2+} \times \frac{Q}{SA} \quad (2)$$

where Pb^{2+} is the concentration of lead in solution, Q is the flow rate of solution and SA is the surface area of reaction, based on the geometry of the sample. The dissolution rates for all scenarios tested in the *in situ* AFM set up were calculated. The unsaturated, $PCO_2=0$, net dissolution rate for 0.0 M, 0.01 M, and 1.0 M NaCl was found to be 1.40×10^{-7} mol/ m^2 /sec, 1.98×10^{-7} mol/ m^2 /sec, and 4.54×10^{-7} mol/ m^2 /sec, respectively. The net dissolution rates for the CO_2 saturated environment were found to be 6.44×10^{-8} mol/ m^2 /sec,, 1.14×10^{-7} mol/ m^2 /sec, and 3.68×10^{-7} mol/ m^2 /sec for the 0.0 M, 0.01 M, and 1.0 M NaCl systems respectively. The dissolution rate data for the *in situ* AFM experiments is summarized in the table below.

Table 3.2 *In situ* Flow-through in AFM fluid cell Dissolution Rates

Net Dissolution Rates (mol/m²/s)					
0M NaCl		0.01M NaCl		1.0M NaCl	
PCO ₂ =0	PCO ₂ =1	PCO ₂ =0	PCO ₂ =1	PCO ₂ =0	PCO ₂ =1
1.40E-07	6.44E-08	1.98E-07	1.14E-07	4.54E-07	3.68E-07

The dissolution rate for the continuous leak experiment involving powdered PbS samples was also calculated for both the CO₂ saturated and unsaturated condition applying a simple batch reactor analysis on the data that is far from equilibrium. The dissolution rate calculations for this scenario were calculated using:

$$R = \frac{\left(\frac{d[Pb^{2+}]}{dt} \right)}{s} \quad (3)$$

where [Pb²⁺] is the total amount of metal (in moles) released from the solid and s is the surface area of the PbS sample. Concentration values at a time of 5 hours, far from equilibrium, were used for to determine dissolution rates and the BET measurement of 1.225 m²/g was available to determine a relevant surface area. The dissolution rate for the CO₂ saturated system was found to be 2.01 × 10⁻⁵ mol/m²/sec and 2.72x10⁻⁵ mol/m²/sec for the unsaturated CO₂ system. The CO₂ saturated systems shows the dissolution rate dropping by nearly half compared to the unsaturated system which is comparable to the *in situ* dissolution rates.

The difference in the net dissolution rates calculated from the *in situ* AFM experiment and the continuous leak experiment are significant. The different in these numbers could be the result of two factors. First, two different methods were used for normalizing the surface area in assessing these rates. The *in situ* AFM calculated the surface area based off the geometry of the sample while the continuous leak experiment utilized the measured BET value for PbS powder. The other reason for this discrepancy may be due to the nature of the PbS sample. The *in situ* AFM experiment is conducted with a crystal sample which is naturally more stable than the powder that is used in the continuous leak experiment. The powder used in the continuous leak experiment is also more likely to dissolve faster since they are smaller particles with more active sites, allowing for greater dissolution.

Precipitation Rate

The precipitation rate occurring on the surface of galena is important to understand the complete process occurring with the interaction between CO₂-H₂O-PbS and coupled

with the overall dissolution rate may provide information on the intrinsic dissolution rate from galena. Precipitation rates for the 1.0 M NaCl, $P_{CO_2}=1$ system where each sample had both sides cleaved along the (100) plane and each sample had a side cleaved along the (100) and (111)/(110) plane were calculated. The precipitation rate for the experiment with both surfaces cleaved along the (100) plane had a precipitation rate of 1.289×10^{-8} mol/m²/sec based on the frequency of precipitation on the surface. The precipitation rate for the experiment with samples cleaved one side along the (100) and one side along the (111)/(110) plane is 7.513×10^{-8} mol/m²/sec. These rates show about a 500% increase in precipitation rate when the surface had at least on side with rough (111)/(110) cleavage.

The net dissolution and precipitation rates can be taken together to provide further information on the intrinsic dissolution rate from PbS. The intrinsic dissolution rate is:

$$\text{Intrinsic Dissolution rate (mol/m}^2\text{/sec)} = \text{Net Dissolution Rate} + \text{Precipitation Rate}$$

Knowing about the precipitation rate can provide more detailed information on how the rate of Pb²⁺ ions' release from the system.

4.3 Surface Plane Reactivity

The reactivity of the different surface planes of galena was also of interest to this report as an understanding of the dissolution of various planes would provide a measure of the impact and importance of such details. To understand if this phenomenon is noticeable on a slightly larger scale is important to assess how important the phenomenon may be. As discussed earlier, there is evidence to suggest greater dissolution on the (111) plane as compared to the (100). This trend is confirmed in our experiments, as evidenced with the *ex situ* experiments. After reaction with CO₂ saturated solutions, the surface of galena specifically cut along the (111) cleavage exhibited more dissolution than the cleaved (100) surface. The *ex situ* experiment involving three different test tubes also confirm this, as the test tubes with samples having a (111)/(110) and (100) cleavage had a much higher frequency of precipitation. This is believed to be the result of an abundance of Pb²⁺ made available from the dissolution of the (111)/(110) phase. The

(111) surface demonstrated more dissolution on the surface because of coordination number of Pb^{2+} in the solid.

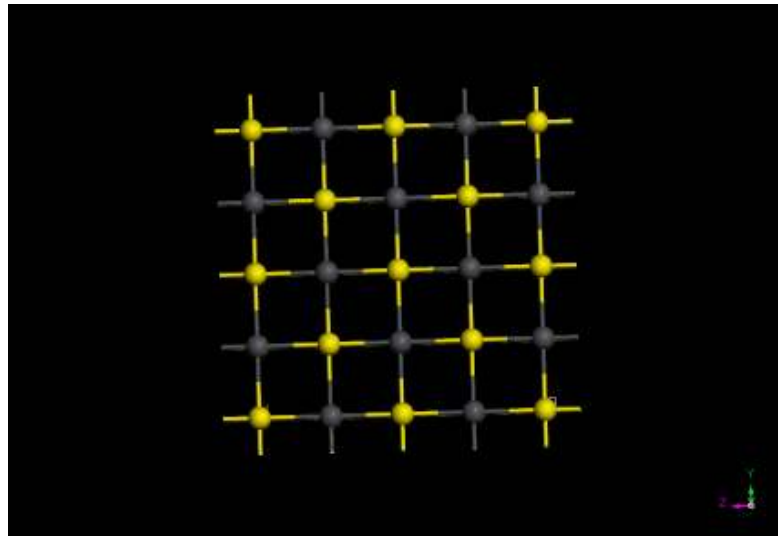


Figure 4.1 (100) Cleavage Plane

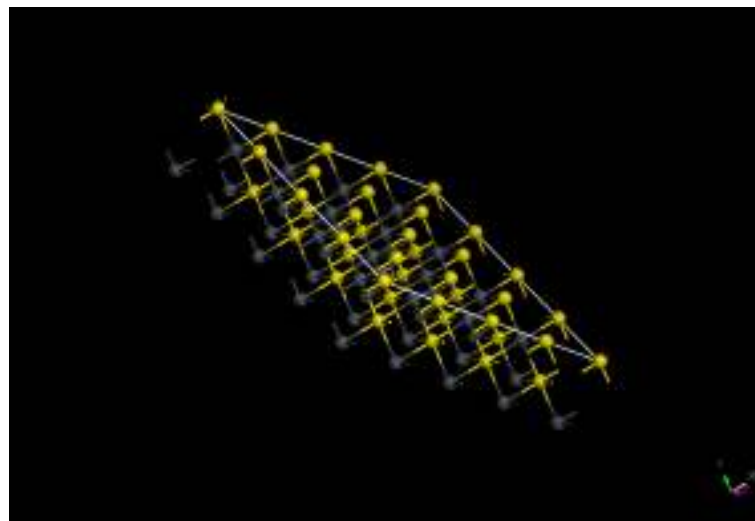


Figure 4.2 (111) Cleavage Plane

The (111) surface has a coordination number of three, filling a kink-link position in the framework of the mineral while the (100) surface has a coordination number of 5, with the atoms occupying a terrace position [47]. This means fewer bonds are holding the Pb^{2+} to the surface in the (111) plane, resulting in the higher reactivity. Surface reactivity of galena is still evident on the millimeter scale and continues to impact the reactions occurring and can lead to higher Pb^{2+} concentrations in solution.

The effect of different surface planes is important because the position of atoms exposed to the aqueous environment plays a fundamental role in how the mineral will react. The dissolution of PbS in acidic solution is most likely controlled by reactions involving negatively-charged sulfide sites [47]. The presence of these sites on different surface planes impact how the reaction mechanism might proceed and highlight why dissolution on the (111)/(110) surface would be enhanced. The balance between favorable kinetic and thermodynamic conditions is important to understand. The removal of ions from the bulk material allows for the formation of a hydration sphere around the ion, resulting in a thermodynamically favorable process [47]. The availability of these sites on different planes will greatly impact the dissolution rate observed for each plane which is important to understanding the release of Pb^{2+} into USDW.

4.4 Precipitation Identification

The identification of precipitation is a very important element to understanding the reactions occurring between galena, water, and CO_2 . Identification of the secondary mineral phase is critical to elucidating the mechanism of the reactions at $\text{PbS-H}_2\text{O-CO}_2$ interactions. FTIR, XPS, and SEM are instrumental provided some information about the precipitation on the surface. FTIR spectra were collected from powdered samples of galena and though there was some difficulty in confirming the identity of the mineral phases present with peak matching only. From the FTIR data, the primary peak changes for the single-leak experiment corresponded to elemental sulfur or Pb(OH)_2 and the primary peak changes for the continuous leak experiment corresponded to PbSO_4 , Pb(OH)_2 , or PbCO_3 . This information is interesting in that the previous literature reported the development of a sulfur film on the surface of galena before reactions leading to other phases on the surface. The single leak experiment seems to agree with this sentiment as there was not a constant source of CO_2 or oxygen to continue to allow the reaction to move forward, resulting in there still being a significant amount of sulfur to be recognized by the FTIR spectra. From the FTIR data, the

continuous leak seemed to contain more surface complexes including PbSO_4 and PbCO_3 , which could imply the constant source of CO_2 allowing for reactions to continue and the formation of these various secondary mineral phases. The XPS helps provide further insight into this system by providing information on the oxidation state and composition of the surface elements. The main changes seen in the XPS analysis focused on the differences in the C and O spectrum. In the unsaturated system, there is evidence of carbonate on the surface and Pb(OH)_2 and PbO ; the saturated system also has evidence of carbonates, Pb(OH)_2 and PbO , but there are also several interesting alterations. First of all, this result is unexpected for the unsaturated system and indicates the potential for reactions occurring in air after reaction, the presence of trace O_2 in our nitrogen gas cylinder, or the need for further cleaning before reaction to remove any initial contamination. The results are also interesting though, in that the peak for carbonate in the CO_2 saturated environment actually decreased from the reference peak, and the C-C peak has an increased intensity, indicating a potential transformation of carbon into aliphatic hydrocarbon bonds [48]. This is consistent with work by Zhang which reported the capability of ZnS colloid to reduce CO_2 under ultraviolet irradiation to produce C-C bonds in a presence of a sulfur hole scavenger [48, 49]. The peaks in the oxygen spectrum also showed significant differences with the sulfite or carbonate peak, assigned to the 531.8 eV, lowering slightly in the CO_2 saturated system and a strong increase in the intensity of the peak at 530.0 eV, corresponding to PbO . The data from the S 2p spectra helps to rule out the likelihood of sulfur species forming on our surface as the potential peak for sulfite or sulfate is likely just noise. These changes indicate the major components formed in the interactions between $\text{PbS-CO}_2\text{-H}_2\text{O}$ could be lead oxide as well as the potential for some carbonate precipitations as well or some combination thereof. Potential secondary minerals phases available from the experimental data could include litharge (PbO , $\log(K_{sp})=12.9$), basic lead carbonate ($\text{PbCO}_3\cdot\text{Pb(OH)}_2$), $\log(K_{sp})=-18.8$), plumbonacrite ($\text{Pb}_3\text{O}(\text{CO}_3)_3(\text{OH})_2$), or shannonite ($\text{Pb}_2\text{O}(\text{CO}_3)$) [50, 51].

SEM images were also helpful in providing more information about the precipitations forming on the surface and the size and shape of these secondary minerals. The SEM

images showed formations in the CO₂ saturated environment that exhibited interesting geometries. The formation of three interesting shapes – cubic-shaped, flatter almost needle-like, and thin rod or wire shapes were found. This information allows for some elimination of potential formations, ruling out cerussite Pb(CO₃) or hydrocerussite Pb₃(CO₃)₂(OH)₂ as their typical structures, orthorhombic-dipyramidal and trigonal-ditrigonal pyramidal respectively, were not observed [52]. The lack of orthorhombic-dipyramidal structures also rules out the possibility of laurionite, PbClOH, as a secondary mineral phase [52].

4.5 Environmental Implications

This work provides useful information on the mineral-water interactions occurring as a result of CO₂ leakage from geologic sequestration. Better understanding of these geochemical reactions provides more accurate information to obtain a holistic view of the entire life-cycle associated with geologic sequestration as well as to better assess the risks of such projects. This study can also help provide information on expected Pb²⁺ concentrations to ensure adequate water quality in underground sources of drinking water. The extent of the release of Pb²⁺ from galena sources in the ground is critically important for human health and safety. This work provides insight as to the effect of CO₂, the reactivity of different surface planes of PbS, and the effect of the high salinity or salt concentrations associated with deep, saline aquifers on the concentration of lead in aqueous solutions. The introduction of CO₂ shows the formations of precipitation on galena's surface and may imply the ability for trapping lead within these secondary mineral phases. This work also has important implications for developing a more accurate reactive transport geochemical modeling. The dissolution and precipitation rates expressed in this work can provide more accurate data for these important simulations as it provides specific values for systems more closely mirroring those of interest in geologic sequestration simulations. The intrinsic dissolution rate may be obtained to provide more accurate information.

Chapter 5

Conclusions & Future Work

This work has provided useful information about the mechanisms and kinetics occurring with the interaction between PbS-H₂O-CO₂ and a better understanding of the potential impact of CO₂ leakage from geological carbon sequestration.

5.1 Conclusion

The relationships between PbS-H₂O-CO₂ are important to study to understand the potential risks associated with geologic carbon sequestration. This work sought to understand several different facets of these interactions, namely the surface reactivity of galena, the dissolution rate, and the influence of the CO₂ leakage source. The dissolution rate was quantified for the *in situ* AFM experiment, and the values were within an order of magnitude of other published results. It was revealed that CO₂ saturated systems had greater reactions resulting in precipitations than the unsaturated system. This was confirmed with Pb²⁺ concentrations; the unsaturated systems consistently have higher levels of Pb²⁺ in solution. It was also reinforced with AFM images that showed the dominant mechanism in the CO₂ saturated environment was precipitations, while the most likely seen formation in the unsaturated system were dissolution pits. The precipitations formed from the introduction of CO₂ were found to be one of the following possibilities: litharge (PbO), basic lead carbonate (PbCO₃·Pb(OH)₂), plumbonacrite (Pb₅O(CO₃)₃(OH)₂), or shannonite (Pb₂O(CO₃)). The surface reactivity of different planes of galena was investigated and the surface reactivity of the (111) surface was shown to be more reactive, resulting in a greater frequency of precipitation when it was in the system. Finally, the impact of a single-leak and continuous-leak was examined. The single-leak experiment was shown to have less

of an impact than the continuous leak, resulting in nearly identical Pb^{2+} concentrations and showing evidence of reactions on the surface progressing to only the initial stage of an elemental sulfur film.

5.2 Future Work

While this work provide critical information to understand the reactions occurring between galena, water, and CO_2 , there are still some unanswered questions regarding the system that could be addressed in future studies. The identification of the precipitation forming on the surface of galena is important work to continue. The ability to identify the three features observed on SEM images would allow for a better understanding of the reaction system and more confident information on what mineral phase is forming. The secondary minerals phase has important implications since understanding the potential forms of lead trapping that may occur will help gauge the risks associated with potential CO_2 leakage from geologic sequestration.

This work yielded very interesting results in regards to the pathway for secondary mineral phase formation, particularly the development of a C-C on the galena surface. The possibility of galena reducing CO_2 into organic compounds is possible as there has been evidence of ZnS reducing CO_2 under ultraviolet radiation.[48] Important future work would be to further investigate this phenomenon in regards to PbS. Future work on this topic also includes a focused effort on elucidating the reaction mechanism and sequences that result in specific secondary mineral phases forming on the surface of galena. Clearly defining precipitations on the surface and determining the various weights and compositions would be very useful in understanding the $\text{PbS-H}_2\text{O-CO}_2$ system.

In regards to geochemical transport simulations, much can be built upon this work. While this work provided useful dissolution rate data for galena to update geochemical models, others minerals containing toxic or harmful metals are present in the ground at geologic sequestration sites. The experimental setup devised in this study can be used

to assess the dissolution rates and study the interactions between minerals with proposed higher sensitivity to CO₂ leakage, most notably arsenopyrite (FeAsS).[53] The flexibility of this setup allows for quick investigations of other minerals of interest to this system. Understanding the dissolution and mobilization of toxic heavy metals is the crucial goal of this research and attainable through the development of geochemical simulations and the quantitative results obtained through experiments such as this.

Another interesting facet of this system important for future work is to study the sulfate concentration. Ion chromatography measurements of the S in the system would allow us to quantify the amount of S and rate of release of this element into the aqueous environment. This information, coupled with the Pb²⁺ concentrations, would allow for a greater understanding of how PbS is interacting with solution and the mechanism for dissolution. This information would provide data that would provide insight into the degree that sulfur controls the dissolution rate. Concentration of S would also enable us to see the relative dissolution rates for Pb and S to see if one element is fast or slow, particularly since there is the potential for galena to form a film of elemental sulfur on the surface. The effect of oxygen concentration on dissolution and precipitation of secondary mineral phases is also an important factor to study further in order to understand the interactions between PbS-CO₂-H₂O.

Molecular modeling of this system is also an interesting endeavor to pursue in future work, particularly relating to the changes observed on the various cleavage planes of galena. An analysis of the different energies found at the (111) and (100) surface could help explain why these surfaces are reacting differently and elucidate or clarify the atomic changes occurring at each surface. It could also provide a way to look at the adsorption of CO₂ onto PbS surface and how the reaction occurs on the molecular level.

Appendix A

Table of References for Peak Matches

An important element to analysis of both the FTIR and XPS runs is the matching of given peaks to reference standards to correctly identify the bonds forming. Tables generated for use in the FTIR and XPS matching are found below.

Table A.1 Peak Matches for FTIR

FTIR peaks	Species	Reference
Wavelength	Species	Reference
1390, broad band between 1370-1400	PbOH	In situ FTIR-Spectroelectrochemical Study of the Anodic Processes on a Galena (PbS) Electrode under Open-Air Conditions in the Absence and Presence of <i>n</i> -Butyl Xanthate
1220, 1110, 1005, 983	lead thiosulfate	In situ FTIR-Spectroelectrochemical Study of the Anodic Processes on a Galena (PbS) Electrode under Open-Air Conditions in the Absence and Presence of <i>n</i> -Butyl Xanthate
950, 960	lead sulfite	In situ FTIR-Spectroelectrochemical Study of the Anodic Processes on a Galena (PbS) Electrode under Open-Air Conditions in the Absence and Presence of <i>n</i> -Butyl Xanthate
1115-1120, 982	PbS ₂ O ₃	Anodic Oxidation of Galena (PbS) Studied FTIR-Spectroelectrochemically
1380, 1050	PbOH, sulfate	Anodic Oxidation of Galena (PbS) Studied FTIR-Spectroelectrochemically
597, 631, 967, 1055, 1171	lead sulfate	FTIR analysis of sulphide mineral surfaces before and after collection: galena
678, 839, 1053, 1401, 1432	lead carbonate	FTIR analysis of sulphide mineral surfaces before and after collection: galena
1020, 1100, 1146, 1220	PbS	FTIR analysis of sulphide mineral surfaces before and after collection: galena
broad band at 960	PbSO ₃	An in situ FTIR study of galena and pyrite oxidation in aqueous solution
660, 1095, 1122	pyrite (Fe ₂ S)	On the growth of colloform textures: a case study of sphalerite from the Galmoy ore body, Ireland
454, 541, 614, 676, 779, 847, 875, 964, 1041, 1091, 1127, 1193, 1257, 1297, 1337, 1381, 1408, 1487, 1584 and 1622	cystine (S-S)	Problem in analyzing cystine stones using FTIR spectroscopy
1120, 580	SO ₄ ²⁻	Investigation on the Mechanism of H ₂ S Removal by Biological Activated Carbon in a Horizontal Biotrickling Filter
1350-1450 (str)	sulfate	http://www.cem.msu.edu/~reusch/VirtTxtJml/Spectrpy/InfraRed/infrared.htm

[54-61]

Table A.2 XPS Matches for XPS

XPS Peaks	Binding Energy	Species	Reference
Pb	137.8	PbS	Effect of conductive BaPbO ₃ electrode on the structural and dielectric properties of (Pb,Ba)ZrO ₃ films
	138.9	PbO	Preparation of PbS-type PbO nanocrystals in a room-temperature ionic liquid
	138.5	PbSO ₃	The Principle of Continuity of Phase Formation at Mineral Surfaces
O	530	PbO	Preparation of PbS-type PbO nanocrystals in a room-temperature ionic liquid
	531.8	PbO, PbSO ₄ , PbCO ₃	The non-oxidative dissolution of galena nanocrystals: Insights into mineral dissolution rates as a function of grain size, shape, and aggregation state
	533.5	attached H ₂ O	Electrochemical behaviour of galena (PbS) in aqueous nitric acid and perchloric acid solutions.
S	161.1	PbS	http://www.artechhouse.com/GetBlob.aspx?strName=Nabok-ch03%20sample%20chapter.pdf
	166.1	PbSO ₃	The Principle of Continuity of Phase Formation at Mineral Surfaces
C	285.2	C-C	Peptide-immobilized nanoporous alumina membranes for enhanced osteoblast adhesion
	286.7	C-C, oxidized C-C	The non-oxidative dissolution of galena nanocrystals: Insights into mineral dissolution rates as a function of grain size, shape, and aggregation state
	288.5	PbCO ₃ PbCO ₃	Characterisation of sphalerite and pyrite flotation samples by XPS and ToF-SIMS Characterisation of sphalerite and pyrite flotation samples by XPS and ToF-SIMS

[35, 40-43, 45, 46, 62]

References

1. Weart, S. *The Discovery of Global Warming*. 2009 [cited 2009 April 15, 2010]; Available from: <http://www.aip.org/history/climate/co2.htm>.
2. IPCC. [cited 2010 4/20/10]; Available from: http://www.ipcc.ch/organization/organization_history.htm.
3. *Methods for Storing CO₂ in Deep Underground Geological Formations*, LBNL: ESD.
4. *Big Sky Carbon Sequestration Partnership*. [cited 2009 March 20]; Available from: <http://www.bigskyco2.org/>.
5. *Midwest Geological Sequestration Consortium*. [cited 2009 March 30]; Available from: <http://www.sequestration.org/>.
6. *Midwest Regional Carbon Sequestration Partnership*. [cited 2009 April 15]; Available from: <http://216.109.210.162/>.
7. *Plains CO₂ Reduction Partnership*. [cited 2009 March 28]; Available from: <http://www.undeerc.org/pcor/>.
8. *Southeast Regional Carbon Sequestration Partnership*. [cited 2009 April 20]; Available from: <http://www.secarbon.org/>.
9. *Southwest Regional Carbon Sequestration Partnership*. [cited March 25 2009]; Available from: <http://www.southwestcarbonpartnership.org/>.
10. *West Coast Regional Carbon Sequestration Partnership*. [cited 2009 April 15]; Available from: <http://www.westcarb.org/>.
11. Bruant, R.G.G., A. J.; Celia, M. A.; Peters, C. A., *Safe storage of CO₂ in deep saline aquifers*. *Environmental Science & Technology*, 2002. **36**(11): p. 240A-245A.
12. Kutchko, B.G.S., B. R.; Lowry, G. V.; Dzombak, D. A.; N., T., *Rate of CO₂ Attack on Hydrated Class H Well Cement under Geologic Sequestration Conditions*. *Environmental Science & Technology*, 2008. **42**: p. 6237-6242.
13. Wang, S. and P.R. Jaffe, *Dissolution of a mineral phase in potable aquifers due to CO₂ releases from deep formations; effect of dissolution kinetics*. *Energy Conversion and Management*, 2004. **45**(18-19): p. 2833-2848.
14. USEPA, *Federal Requirements Under the Underground Injection Control (UIC) Program for Carbon Dioxide (CO₂) Geologic Sequestration (GS) Wells; Proposed Rule*. *Federal Register*, July 25, 2008. **73**(144): p. 43492-43541.
15. Bandza, A.J. and S.P. Vajjhala, *Long-Term Risks and Short-Term Regulations: Modeling the Transition from Enhanced Oil Recovery to Geologic Carbon Sequestration*. RFF Discussion, 2008: p. Paper No. 08-29, <http://ssrn.com/abstract=1272668>.
16. Nelson, C.R.E., J. M.; Sorensen, J. A.; Steadman, E. N. *Factors affecting the potential for CO₂ leakage from geologic sinks*. 2005.

17. DOE Carbon Sequestration Technology Roadmap and Program Plan. US Department of Energy 2007.
18. Grogan, R.M., Bradbury, James C., "Fluorite-zinc-lead deposits of the Illinois-Kentucky mining district", in *Ore Deposits in the United States*. 1968, American Institute of Mining, Metallurgical, and Petroleum Engineers (AIME): New York. p. 370-399.
19. Galena. 2010 [cited 2010 May 3]; Available from: <http://en.wikipedia.org/wiki/Galena>.
20. Energy, U.D.o., *An Assessment of Geologic Sequestration Options in the Illinois Basin*. 2005.
21. Kehew, A.E., *Applied Chemical Hydrogeology*. 2001, Upper Saddle River, NJ 07458: Prentice Hall.
22. *Drinking Water Contaminants: List of Contaminant and the MCL's*. 2009 September 11, 2009 [cited 2009 December 10].
23. Xu, T., et al., *TOUGHREACT--A simulation program for non-isothermal multiphase reactive geochemical transport in variably saturated geologic media: Applications to geothermal injectivity and CO₂ geological sequestration*. *Computers & Geosciences*, 2006. **32**(2): p. 145-165.
24. Zheng, L., et al., *Reactive transport simulations to study groundwater quality changes in response to CO₂ leakage from deep geological storage*. *Energy Procedia*, 2009. **1**(1): p. 1887-1894.
25. Unger, C.M.O.a.A.J.A., *On Leakage and Seepage from Geologic Carbon Sequestration Sites*. *Vadose Zone Journal*, 2003. **2**: p. 289-296.
26. Bachu, S., *Sequestration of CO₂ in geological media: criteria and approach for site selection in response to climate change*. *Energy Conversion and Management*, 2000. **41**(9): p. 953-970.
27. Zhang, W., Li, Y., Xu, T., Qiang, W., Xiao, S., *The effects of carbon dioxide leakage on fractures, and water quality of potable aquifers during geological sequestration of CO₂*. *Chinese Journal of Geochemistry*, 2006. **25**: p. 58.
28. Wright, K., et al., *Cluster models of the dissociation of water on the surface of galena (PbS)*. *Chemical Physics Letters*, 1999. **299**(6): p. 527-531.
29. Zhang, S., et al., *Dissolution kinetics of galena in acid NaCl solutions at 25--75 °C*. *Applied Geochemistry*, 2004. **19**(6): p. 835-841.
30. Kim, B.S., et al., *Scanning Tunneling Microscopy Studies of Galena: The Mechanisms of Oxidation in Aqueous Solution*. *Langmuir*, 1995. **11**(7): p. 2554-2562.
31. Gerson, A.R. and A.R. O'Dea, *A quantum chemical investigation of the oxidation and dissolution mechanisms of Galena*. *Geochimica et Cosmochimica Acta*, 2003. **67**(5): p. 813-822.
32. Scheetz, C.D., *Dissolution, Transport, and Fate of Lead on Shooting Ranges*, in *Geological Sciences*. 2004, University of Virginia: Blacksburg. p. 47.
33. Nowak, P. and K. Laajalehto, *Oxidation of galena surface - an XPS study of the formation of sulfoxy species*. *Applied Surface Science*, 2000. **157**(3): p. 101-111.

34. Cama, J., et al., *Galena surface reactivity at acidic pH and 25 °C based on flow-through and in situ AFM experiments*. *Chemical Geology*, 2005. **214**(3-4): p. 309-330.
35. Liu, J., et al., *The non-oxidative dissolution of galena nanocrystals: Insights into mineral dissolution rates as a function of grain size, shape, and aggregation state*. *Geochimica et Cosmochimica Acta*, 2008. **72**(24): p. 5984-5996.
36. Becker, U., K.M. Rosso, and M.F. Hochella, *The proximity effect on semiconducting mineral surfaces: a new aspect of mineral surface reactivity and surface complexation theory?* *Geochimica et Cosmochimica Acta*, 2001. **65**(16): p. 2641-2649.
37. Giovanni De Giudici, P.R., Pierfranco Lattanzi, and Alberto Anedda, *Dissolution of the (001) surface of galena: An in situ assessment of surface speciation by fluid-cell micro-Raman spectroscopy*. *American Mineralogist*, 2007. **92**: p. 518-524.
38. Jun, Y.S.M., S. T., *Microscopic observations of reductive manganite dissolution under oxic conditions*. *Environmental Science & Technology*, 2003. **37**(11): p. 2363-2370.
39. Steff, *Schema MEB*. 2010. p. Diagram of a scanning electron microscope with English captions.
40. Li Juan, C., et al., *Preparation of PbS-type PbO nanocrystals in a room-temperature ionic liquid*. *Materials Letters*, 2005. **59**(24-25): p. 3119-3121.
41. Wu, L.-J.W.a.J.-M., *Effect of conductive BaPbO₃ electrode on the structural and dielectric properties of (Pb,Ba)ZrO₃ films*. *Journal of Physics D: Applied Physics*, 2007. **40**(15): p. 4707.
42. Tauson, V.L., *The principle of continuity of phase formation at mineral surfaces*. *Doklady Earth Sciences*, 2009. **425**(2): p. 471-475.
43. Nabok, A., *Structural Study of Organic/Inorganic Nanocomposites*, Artech House: Norwood, Massachusetts.
44. Leary Swan, E.E., K.C. Popat, and T.A. Desai, *Peptide-immobilized nanoporous alumina membranes for enhanced osteoblast adhesion*. *Biomaterials*, 2005. **26**(14): p. 1969-1976.
45. Boulton, A., D. Fornasiero, and J. Ralston, *Characterisation of sphalerite and pyrite flotation samples by XPS and ToF-SIMS*. *International Journal of Mineral Processing*, 2003. **70**(1-4): p. 205-219.
46. Paul, R.L., et al., *The electrochemical behaviour of galena (lead sulphide) -- I. Anodic dissolution*. *Electrochimica Acta*, 1978. **23**(7): p. 625-633.
47. Higgins, S.R. and R.J. Hamers, *Chemical dissolution of the galena (001) surface observed using electrochemical scanning tunneling microscopy*. *Geochimica et Cosmochimica Acta*, 1996. **60**(16): p. 3067-3073.
48. Zhang, X.V., et al., *Photodriven reduction and oxidation reactions on colloidal semiconductor particles: Implications for prebiotic synthesis*. *Journal of Photochemistry and Photobiology A: Chemistry*, 2007. **185**(2-3): p. 301-311.

49. Xiang V. Zhang, S.T.M., *Driving Parts of the Krebs Cycle in Reverse through Mineral Photochemistry*. JACS Communications, 2006. **128**: p. 16032-16033.
50. S. V. Krivovichev, a.P.C.B., *Crystal chemistry of basic lead carbonates. I. Crystal structure of synthetic shannonite, Pb₂O(CO₃)*. Mineralogical Magazine, 2000. **64**(6): p. 1063-1068.
51. Roberts, A.C., et al., *Shannonite, Pb₂OCO₃, A new mineral from the Grand-Reef-Mine, Graham County, Arizona, USA*. Mineralogical Magazine, 1995. **59**(395): p. 305-310.
52. Dermatas D., D., M., Dutko, P., Menouno N., Arienti P., Shen, G., *Weathering of Lead in Fort Irwin Firing Range Soils*. Global Nest: The International Journal, 2004. **6**(2): p. 167-175.
53. Zheng, L., et al., *On mobilization of lead and arsenic in groundwater in response to CO₂ leakage from deep geological storage*. Chemical Geology, 2009. **268**(3-4): p. 281-297.
54. Chernyshova, I.V., *In Situ FTIR–Spectroelectrochemical Study of the Anodic Processes on a Galena (PbS) Electrode under Open-Air Conditions in the Absence and Presence of n-Butyl Xanthate*. Langmuir, 2002. **18**(18): p. 6962-6968.
55. Chernyshova, I.V., *Anodic Oxidation of Galena (PbS) Studied FTIR-Spectroelectrochemically*. Journal of Physical Chemistry B., 2001. **105**(34): p. 8178-8184.
56. Cases, J.M. and P. De Donato, *FTIR analysis of sulphide mineral surfaces before and after collection: galena*. International Journal of Mineral Processing, 1991. **33**(1-4): p. 49-65.
57. Chernyshova, I.V., *An in situ FTIR study of galena and pyrite oxidation in aqueous solution*. Journal of Electroanalytical Chemistry, 2003. **558**: p. 83-98.
58. Craig D. Barrie, A.J.B., Alan P. Boyle, Patrick J. Williams, Kevin Blake, Jamie J. Wilkinson, Mike Lowther, Paul McDermott & David J. Prior, *On the growth of colloform textures: a case study of sphalerite from the Galmoy ore body, Ireland*. Journal of the Geological Society, 2009. **166**(3): p. 563-582.
59. Y. M. Fazil Marickar, P.R.L., Luxmi Varma and Peter Koshy, *Problem in analyzing cystine stones using FTIR spectroscopy*. Urological Research, 2009. **37**(5): p. 263-269.
60. Huiqi Duan, R.Y.a.L.C.C.K., *Investigation on the mechanism of H₂S removal by biological activated carbon in a horizontal biotrickling filter*. Applied Microbiology and Biotechnology, 2005. **69**(3): p. 350-357.
61. *Infrared Spectroscopy*. [cited 2010 4/22]; Available from: <http://www.cem.msu.edu/~reusch/VirtTxtJml/Spectrpy/InfraRed/infrared.htm>
62. Yu. Mikhlin, A.K., E. Mikhlina, V. Kargin and I. Asanov, *Electrochemical behaviour of galena (PbS) in aqueous nitric acid and perchloric acid solutions*. Journal of Applied Electrochemistry, 2004. **34**(1): p. 37-46.

Vita

Kathleen O'Malley

Date of Birth	April 27, 1987
Place of Birth	Houston, Texas
Degrees	B.S. Chemical Engineering, May 2010 M.S. Chemical Engineering, May 2010
Professional Societies	American Institute of Chemical Engineers Society of Hispanic Professional Engineers American Chemical Society
Scholarships	Annika Rodriguez Scholarship Enterprise Rent-a-Car Scholarship Joseph Puleo Memorial Scholarship
Activities & Awards	Mid-America Environmental Engineering Conference (FL 2009) -Talk at Washington University in Saint Louis American Chemical Society National Meeting (SP 2010) -Poster presentation in Geochemistry Division -Poster presentation at WCC Luncheon 2010 ACS WCC/Eli Lilly Travel Grant Award Winner Graduate Mentor – MO STARS Program (SU 2009)

May 2010

PbS-H₂O-CO₂ Interactions in Acidic Salt Solutions, O'Malley, M.S. 2010